REPORT 1244

FREE-STREAM BOUNDARIES OF TURBULENT FLOWS[1]

By Stanley Corrsin and Alan L. Kistler

SUMMARY

An experimental and theoretical study has been made of the instantaneously sharp and irregular front which is always found to separate turbulent fluid from contiguous "nonturbulent" fluid at a free-stream boundary. This distinct demarcation is known to give an intermittent character to hot-wire signals in the boundary zone.

The overall behavior of the front is described statistically in terms of its wrinkle-amplitude growth and its lateral propagation relative to the fluid as functions of downstream coordinate.

It is proposed and justified that the front actually consists of a very thin fluid layer in which direct viscous forces play the central role of transmitting mean and fluctuating vorticity to previously nonturbulent fluid. Outside this "laminar superlayer" there is presumably a field of irrotational velocity fluctuations (the "nonturbulent" flow) with constant mean velocity. As outlined in the following paragraphs, theoretical analysis based on this general physical picture gives results on front behavior which are in plausible agreement with experimental results for three turbulent shear flows: rough-wall boundary layer, plane wake, and round jet.

It is shown that the rate of increase of wrinkle amplitude of the front can be roughly explained as a Lagrangian diffusion process, using the statistical properties of the turbulence in the fully turbulent zone.

The transversal propagation velocity of the turbulence front is predicted by the behavior of a physicomathematical model of the laminar superlayer. The model is a generalized Stokes-Rayleigh infinite wall, oscillating in its own plane, translating to give constant mean vorticity at the boundary, plus local vorticity production and uniform suction velocity.

Finally, various statistical properties of the turbulence front location as a stationary random variable (for fixed downstream position) have been either directly measured or indirectly inferred from known theorems on Gaussian stochastic processes; it is found that for boundary layer, wake, and jet the front location is very nearly Gaussian. Specifically, it is possible, therefore, to estimate the autocorrelation function of the front position.

INTRODUCTION

Until the last few years, basic experimental and (especially) theoretical attacks upon the problems of turbulent flow have centered on fully turbulent fields, both isotropic and shearing. The experimental researches have been concerned with the measurement of significant statistical quantities with the hope that these will give some insight into the mechanism of fully developed turbulence and might even suggest a profitable theoretical approach.

In reality, however, every turbulent flow is bounded by fluid not in a turbulent state. If the boundary spacings can be made very large compared with the characteristic correlation lengths of the turbulence, for example, integral scale and dissipative scale (microscale), then an "infinite field" approximation can be used. This has been possible in research on the decaying turbulence behind regular grids, a reasonably good likeness of Taylor's ideal concept of isotropic turbulence (ref. 1).

It now seems probable that the classic turbulent shear flows, boundary layer, wake, jet, channel, and so forth have transversal integral scales not very small compared with their characteristic widths. This has been shown experimentally for the round jet (ref. 2), the plane half jet (ref. 3), the boundary layer (ref. 4), and the channel (ref. 5). This implies that the general behavior of these shear flows cannot be fully inferred on a (still unsolved) homogeneous shear flow basis but must involve the boundary phenomena.

Turbulent shear flow boundaries can be classified in various ways. A conventional one is the division into (a) solid and (b) free (or free stream) boundaries, depending upon the presence or absence of a solid wall and excluding possible symmetry planes from consideration as boundaries.

A further subdivision can be made in each class according to whether the outside flow or wall is traveling faster or slower than the turbulent fluid just inside the boundary, but this distinction is probably only a quantitative one (because of the nonlinearity of the system), not affecting the nature of the boundary phenomena; a comparison of wake and jet boundaries would illustrate this remark. One can also visualize a boundary state in which this mean velocity difference is zero, that is, the case of uniform velocity field including both turbulent and outside flow.

This investigation is concerned solely with the free boundary condition. In practice, this case generally involves a mean shear stress in the fully turbulent region, reducing

[1] Supersedes NACA TN 3133, "The Free-Stream Boundaries of Turbulent Flows" by Stanley Corrsin and Alan L. Kistler, 1954.

to zero monotonically toward the nonturbulent[2] free-stream flow.

The outstanding observable characteristic of free boundaries is the relatively sharp instantaneous demarcation surface between turbulent and nonturbulent fluid. This shows up very clearly, for example, in short-duration shadowgraphs of the turbulent wakes behind high-speed projectiles (fig. 1). The sharpness of the irregular boundary illustrated persists as far downstream as pictures have been taken, about several hundred wake diameters.

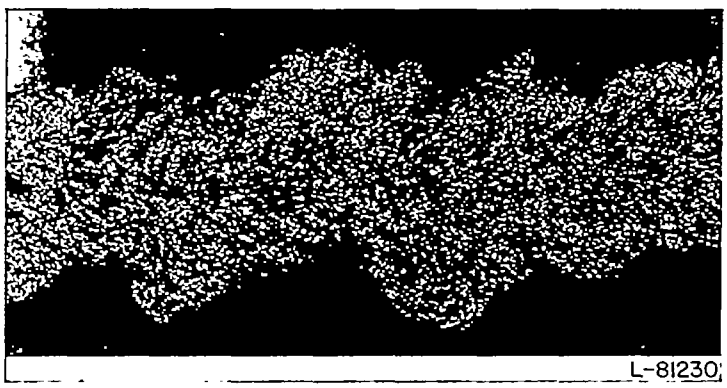

FIGURE 1.—Turbulent wake of bullet. (Courtesy of Ballistic Research Laboratories, Aberdeen Proving Ground.)

In a mixed flow zone of this type, a probe stationary relative to the disturbance (e. g., the wall in a turbulent boundary layer) will be swept over by successive sections of turbulent and nonturbulent fluid. With a hot-wire anemometer this yields an intermittent signal of the type which led to the discovery of this characteristic of free turbulent boundaries (ref. 2). The relative time spent by the probe in turbulent fluid was first measured by Townsend (ref. 6) and called the intermittency factor γ.

Most steady-state shear zones spread with increasing downstream distance. Therefore, there cannot be even rough overall flow similarity unless the average lateral position and the wrinkle amplitude of the sharp boundary both increase at roughly the same rate as does the momentum width of the shear flow. Since it is well known that most "simple" turbulent shear flows exhibit a rough overall similarity, it can immediately be anticipated that this turbulence front must (a) propagate relative to the local fluid in the same sense that a flame front propagates through a combustible mixture and (b) increase its geometrical amplitude with increasing downstream coordinate.

The explanations of these necessary properties of the turbulence front are two of the explicit purposes of this investigation. The two properties are to be measured and to be analytically related to physical properties of the turbulence in the fully turbulent zone.

For any x-station, the intermittency factor $\gamma(y)$ is just 1 minus the distribution function of $Y(t)$, the instantaneous location of the sharp front between turbulent and nonturbulent fluid. For a fixed value of x, $Y(t)$ is a stationary random variable, and

$$\gamma(y) = \text{prob}[y \leqq Y(t) \leqq \infty] \tag{1}$$

Since $\gamma(y)$ is differentiable (in fact, nondifferentiable functions cannot be experimentally so identified), $\partial\gamma/\partial y$ is the probability density of $Y(t)$.

A priori the fact that the free turbulence boundary (vorticity fluctuation boundary according to the physical picture proposed here) remains sharp can be attributed to the continuous irregular stretching of the local vorticity gradient in the boundary, that is, to the fact that the vorticity propagation process is nonlinear; for a given stretching rate, the production of new vorticity is proportional to the amount already present. This must be balanced on the average by the viscous diffusion of the vorticity gradient at the front.

It is obvious that the random vorticity field ordinarily called turbulence can propagate only by direct contact, as opposed to action at a distance, because rotation can be transmitted to irrotational flow only through direct viscous shearing action. This insures that under ordinary circumstances the turbulence front will always be a continuous surface; there will be no islands of turbulence out in the free stream disconnected from the main body of turbulent fluid.

The analytical estimates will include a hypothetical case in which the turbulent part of the flow field is also without shear. This is perhaps the simplest conceivable case under which turbulence propagates into nonturbulent fluid—provided that one can neglect the necessary monotonic time decreases in turbulent energy per unit mass. Under these conditions it is proposed that the distinction between turbulent and nonturbulent zones is the presence or absence, respectively, of random vorticity fluctuations.

A more complex case is the one ordinarily encountered in practice, as described before: a shearing turbulence encroaching on a nonshearing (irrotational) nonturbulent fluid. In this case, the average propagation velocity of the turbulence front should also depend upon the mean shear stress in the turbulent fluid near the front.

A somewhat different situtation, not included fully in the above classes, occurs in the transitional spreading of a turbulent shear region into a shearing laminar region, when the principal shear planes of laminar and turbulent flows are parallel to each other but perpendicular to the mean propagation front.

Such a phenomenon was first studied experimentally by Charters (ref. 7), who called it "transition by transverse contamination." Emmons (ref. 8) has given good experimental evidence that transition from laminar to turbulent flow may often occur in this way, usually from irregularly generated "ignition" spots in the moving fluid, and a preliminary analytical discussion of the turbulence spread under these conditions has been given by Mitchner (ref. 9). However, it appears that Mitchner has omitted from his nonturbulent region the very shear which distinguishes the transition problem. It is not intended that this important case be included in the present report. Although some of the same phenomena may occur as in the simpler nonshear boundary, it is possible that the dominant turbulence propa-

[2] The term "laminar" is reserved for a nonturbulent flow in shear, that is, where viscous forces are important. This is in contrast with the terminology introduced in reference 2, where laminar was used to indicate any nonturbulent flow. Of course, in practice, a "nonturbulent" flow may be one whose turbulence level is much lower than that of the contiguous turbulent flow.

gation mechanism is different. In particular, it may be that a destabilization of the already rotational flow occurs in addition to a transmission of random vorticity by direct viscous action at the turbulent-laminar interface.

When the present work was begun, it was hoped that the problem of propagation of turbulence into a nonturbulent flow could be studied at the boundary between a grid-generated isotropic turbulence and a nonturbulent flow moving at the same uniform speed. This would eliminate the shear stress entirely, although involving a relatively rapid turbulence-level change due to viscous dissipation with no turbulent energy production.

The principal generating arrangement tried was a half grid consisting of a conventional 1-inch-mesh, ¼-inch-dowel grid covering half the tunnel cross section, with a fine mesh screen of virtually identical static-pressure drop covering the other half. Unfortunately, anomalous boundary behavior, arising from complexities in the flow around the joint between grid and screen, could not be eliminated with a reasonable amount of effort. Therefore, the turbulence propagation has been studied in situ, chiefly at the outer edge of a low-speed turbulent boundary layer, with a few measurements in a round jet for an additional check of some particular phenomena. For completeness, some of Townsend's plane-wake data (ref. 10) have also been analyzed in the light of this investigation.

The general purpose of this investigation has been to measure statistical properties of the propagating turbulence front to permit qualitative or even rough quantitative theoretical explanation of the phenomenon.

The work has been carried out at the Department of Aeronautics of The Johns Hopkins University with the financial assistance and sponsorship of the National Advisory Committee for Aeronautics. The authors would like to acknowledge the assistance of Miss Vivian O'Brien, Mr. Aristoteles Scoledes, Mr. Donald Johnson, and Miss M. Ann Emmart as well as the critical advice of Dr. Francis H. Clauser and Dr. Mark V. Morkovin.

SYMBOLS

A	characteristic ordinate in sketch (d)
a	random variable representing some flow property
a_T	same property, taken in turbulent flow only
B	constant
b	random on-off signal, taken between zero and 1
C, D	random variables
c_f	skin friction coefficient, $\frac{\tau_o}{\frac{\rho}{2}\overline{U}_\infty^2}$
d	diameter of rod used to produce plane wake
F_c, F_a, F_{a_T}, F_b	power spectra
G	scalar function
h	height of wall roughness
I	random variable
K	parameter in model of laminar superlayer, equivalent to vortex stretching rate
k	wave number
L	transversal Eulerian scale
L_t	Lagrangian time scale
L_L	Lagrangian length scale, $v'L_t$
l_1, l_2	average pulse lengths of intermittent signal
M	empirical constant
m	exponent of boundary-layer power-law velocity profile
N_I	average frequency of occurrence of any particular value of random variable $I(t)$
N_Y, N_0	average frequency of occurrence of Y and zero, respectively, in front-location variable $Y(t)$
n	cyclic frequency
P	total static pressure
p_1, p_2	probability densities of turbulent and potential segment lengths, respectively, in intermittent signal
$\underline{Q}$	total velocity vector
$\underline{q}$	velocity fluctuation vector, $\underline{Q}-\overline{\underline{Q}}$
q	dynamic pressure in free stream of wind tunnel
R	instantaneous radial location of turbulence front in round jet
R_L	Lagrangian correlation function
R_{uv}	shear correlation coefficient, $\overline{uv}/u'v'$
$R_e, {}_1R_e, {}_2R_e$	Reynolds numbers of laminar superlayer
R_λ	turbulence Reynolds number, $u'\lambda/\nu$
$\underline{r}$	coordinate vector
r	radial coordinate in round jet
r_o	jet orifice radius
$r_{1/2}$	radial position at which $\overline{U}=\frac{1}{2}\overline{U}_{max}$ at a section of the jet
$\underline{S}$	total shear force vector (per unit area) at turbulent side of superlayer, lying in plane of superlayer
$\underline{s}=\underline{S}-\overline{\underline{S}}$	
$T_1\ T_2$	segment (or pulse) lengths of turbulent and potential signal, respectively, in intermittent signal
t	time
U, V, W	velocity along x, y, and z, respectively
$U_i \equiv \underline{Q}$	
$\overline{U}_o$	mean velocity on axis of jet or wake
$\overline{U}_\infty$	mean velocity in free stream of boundary layer or wake
U_τ	skin friction velocity, $\sqrt{\tau_o/\rho}$
u,v,w	velocity fluctuation along x, y, and z, respectively
$u_i \equiv \underline{q}$	
$\overline{V}^*$	average velocity of propagation of turbulence front relative to fluid (perpendicular to its own plane)
x,y,z	Cartesian coordinates (x is measured from beginning of working section in boundary-layer case)
x_1,y_1,z_1	Cartesian coordinates alined locally with turbulence front
$x_i \equiv \underline{r}$	

x_o apparent origin of wake, boundary layer, or jet

Y instantaneous y—location of turbulence front for boundary layer and wake

$Y_1 = Y - \overline{Y}$

Y_w instantaneous y_w—location of turbulence front of plane-wake

$y_w = \frac{y\, d^{-1/2}}{(x-x_o)^{1/2}}$ in wake

$y_{1/2}$ value of y at which mean velocity defect is half maximum

α, β radian frequency of wall oscillation in model of laminer superlayer

γ intermittency factor, relative time spent by a fixed probe in turbulent fluid

$\underline{\Delta}$ instantaneous vector velocity jump across laminar superlayer

δ boundary-layer thickness, the value of y at which $\overline{U} \doteq \overline{U}_\infty$

δ^* boundary-layer displacement thickness

ϵ thickness of laminar superlayer

ϵ_1, ϵ_2 model superlayer thickness for mean and fluctuating vorticity, respectively

θ momentum thickness of boundary layer

Λ_L Lagrangian length scale in flow direction, $\overline{U} L_t$

λ transversal Eulerian microscale of turbulence

λ_t Lagrangian time microscale

λ_Y microscale of $Y(t)$ times $\overline{U}_\infty$

λ_η Lagrangian length microscale, $v'\lambda_t$

μ viscosity coefficient

ν kinematic viscosity coefficient, μ/ρ

Ξ, Z total vorticity components in $x-$ and $z-$ directions, respectively

Ξ_t total vorticity, $\Xi \equiv \underline{\Omega}$

ξ, η, ζ vorticity fluctuation components along x, y, and z, respectively

ξ_t vorticity fluctuation, $\xi_t \equiv \underline{\omega} = \underline{\Omega} - \overline{\underline{\Omega}}$

ρ density

$\sigma = \sqrt{\overline{(Y-\overline{Y})^2}} = \sqrt{\overline{Y_1^2}}$ standard deviation of $(Y - \overline{Y}) \equiv Y_1$

σ_{ik} stress tensor

$\sigma_w = \sqrt{\overline{(Y_w - \overline{Y}_w)^2}}$

τ time interval

τ_o skin friction stress

Φ rate of dissipation of turbulent energy per unit mass of fluid

χ Kolmogoroff (minimum) length, $\chi \equiv (\nu^3/\Phi)^{1/4}$

ψ autocorrelation function of $Y_1(t)$

$\psi_a, \psi_{a_T}, \psi_b$ autocorrelation functions of a, a_T, and b

ψ_c autocorrelation function of trigger output

$\underline{\Omega}$ total vorticity vector

$\underline{\omega}$ vorticity fluctuation vector

Operators:

$\overline{(\ )}$ average

$\tilde{(\ )}$ "short" time or space average

$(\ )' \equiv \sqrt{\overline{(\ )^2}}$ root mean square

$(\ )_T$ hypothetical variable equal to actual variable in turbulent fluid only and obtained by deleting potential fluid part of an intermittent oscillogram

EXPERIMENTAL EQUIPMENT AND PROCEDURES

AERODYNAMIC EQUIPMENT

The wind tunnel (fig. 2) is an open-return NPL type with a 2- by 2-foot working section and a free-stream turbulence level at entrance of $u'/\overline{U} = 0.05$ percent and $v'/\overline{U} = 0.06$ percent at a mean velocity of $\overline{U} = 26$ feet per second.

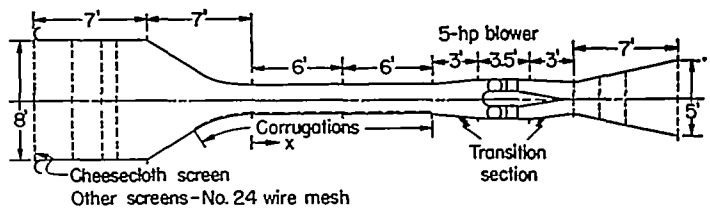

FIGURE 2.—Schematic diagram of wind tunnel.

In order to have a reasonably thick turbulent boundary layer in the relatively short working section, a wall was used as a working surface, and it was roughened by corrugated paper starting from the beginning of the contraction. The corrugations, set perpendicular to the flow, were roughly sinusoidal, with about ½-inch wave length and 5/64-inch amplitude (half height).

The extent of two-dimensionality in the boundary-layer flow was checked by mean velocity profiles at several stations across the 2-foot width of the working surface, at the farthest downstream station, $x = 102$ inches. The uniform zone was 18 inches wide, with a boundary-layer thickness of $\delta \approx 3$ inches from wall to free-stream and, estimating from reference 4, the transversal Eulerian scale was about 0.5 inch.

The boundary-layer measurements were all made at a free-stream velocity of 37 feet per second. The static pressure was very nearly constant along the working section (fig. 3). From comparisons with earlier work on this type of flow (ref. 11), it appears that the flow state is such as to have a fully rough wall condition.

The round-jet unit is sketched schematically in figure 4. The orifice diameter was ½ inch and it was run at an exit velocity of 300 feet per second.

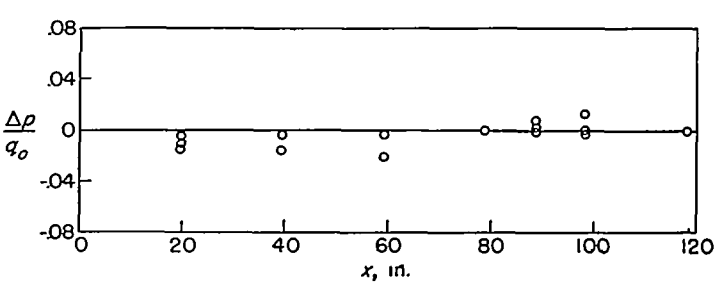

FIGURE 3.—Static-pressure distribution along wind-tunnel working section. q_o, dynamic pressure in free stream at $x = 0$.

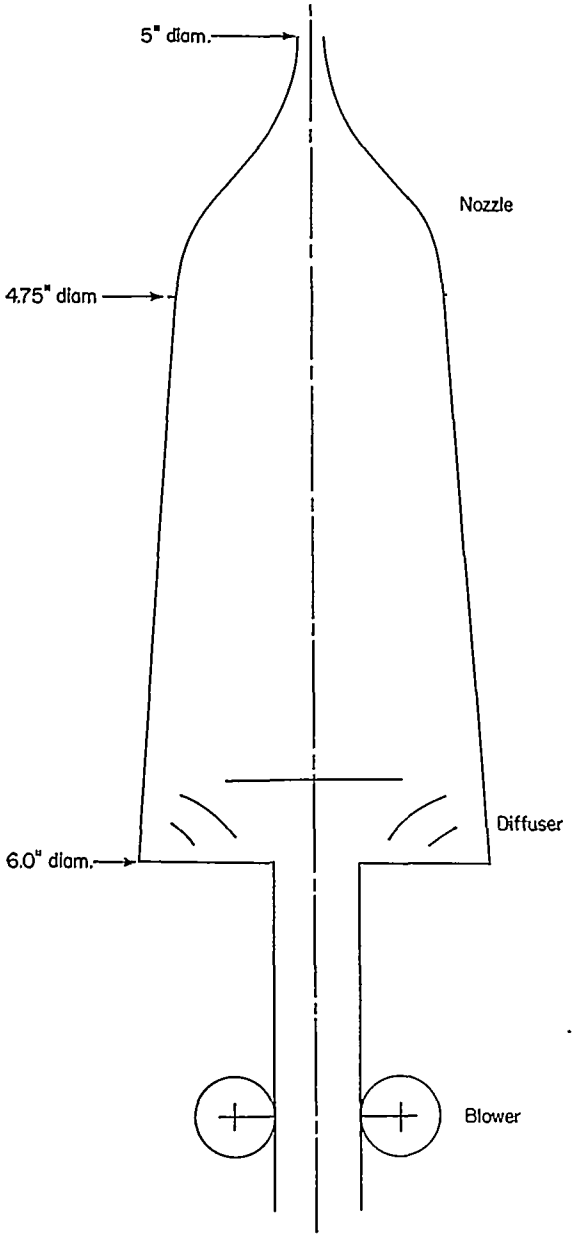

FIGURE 4.—Schematic diagram of round-jet equipment.

HOT-WIRE SET

Most of the measurements reported here were made with the hot-wire anemometer as sensing element. The basic amplifier and compensation unit, constructed by Mr. C. L. Thiele, is described in reference 12. The oscillograms were taken with a General Radio Type 761 camera photographing blue cathode-ray tubes. Measurements of the statistical distribution of lengths of turbulent bursts were made by scaling directly from the recorded oscillograms.

The power spectra were measured with a Hewlett-Packard Type 300A wave analyzer, followed by a vacuum thermocouple. The strongly fluctuating output was averaged by integrating with a fluxmeter and bucking circuit as illustrated in reference 12.

The hot-wires used were either 0.00010 inch platinum or 0.00015 inch tungsten, with lengths of about 1.5 millimeters for the u-meters and 2 millimeters for the X-meters used to measure v', w', and $\overline{uv}$. No correction was applied for finite wire length.

413672—57——66

MEASUREMENT OF INTERMITTENCY

Following Townsend (ref. 6) the intermittency γ is defined as the fractional time spent by the (fixed) probe in turbulent fluid. Townsend has measured γ in two ways: (a) from the "flattening factor" (or "kurtosis") of the probability density of the intermittent signal (ref. 6); (b) from the mean-square output of an on-off signal triggered by passing the intermittent signal through a gate (ref. 10). The method used here is a development of (b), the relative "on time" being measured by counting a high-frequency pulse signal as modulated by the on-off signal. This should give more accurate results at low values of γ.

The overall block diagram is given in figure 5. Figure 6 is a further breakdown of the manipulative details, with a schematic diagram of a hypothetical signal as modified by passage through the various blocks. The actual circuit of this is given in figure 7. It is clear from figure 6 that the number of pulses counted for a given input signal will be a monotonically increasing function of discriminator setting. One would like to find a wide range of discriminator settings over which the count rate, for a given input signal, would be unchanged. Unfortunately, there is no such indication

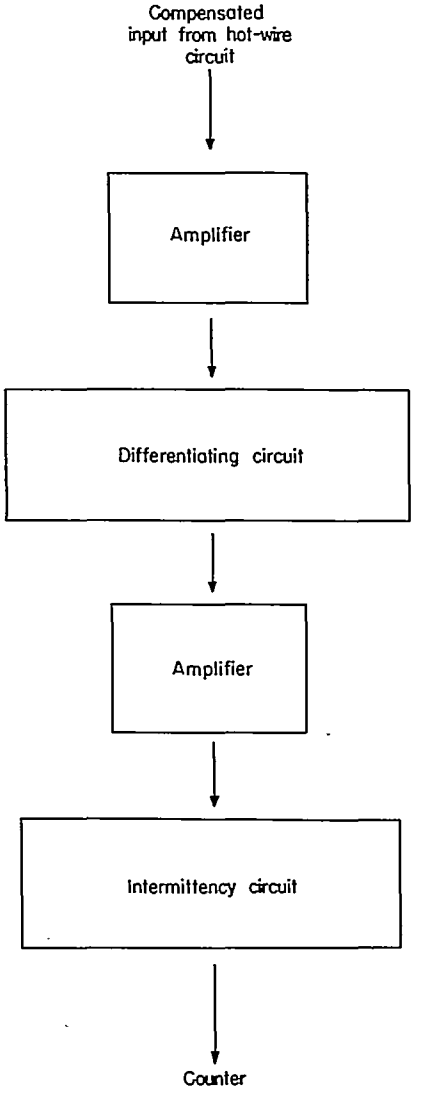

FIGURE 5.—Overall block diagram of intermittency-measuring arrangement.

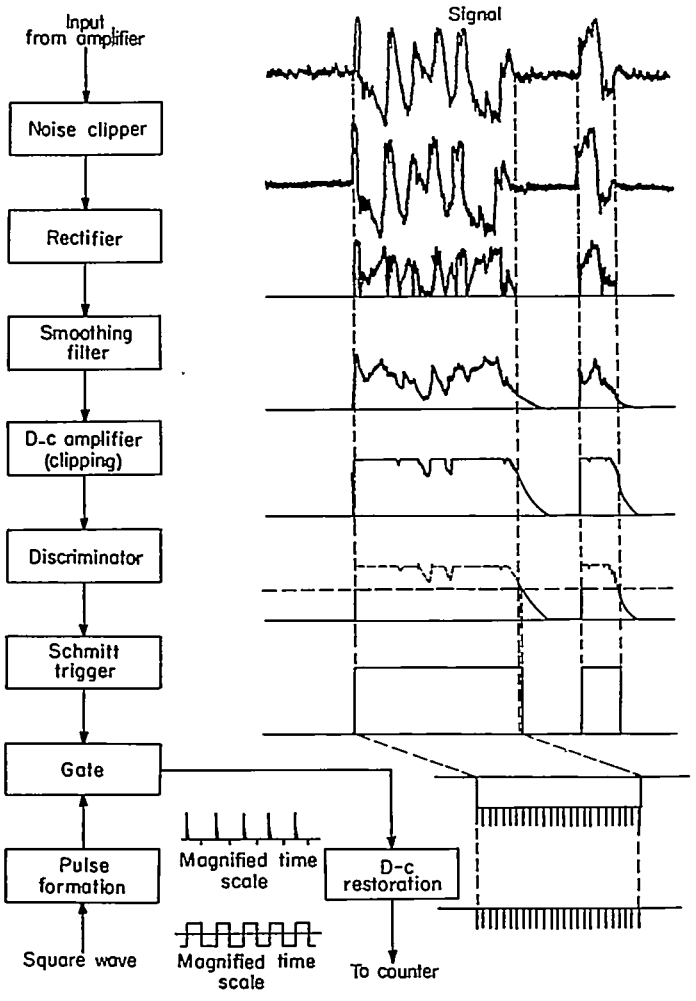

FIGURE 6.—Detailed block diagram of intermittency-measuring device.

of a "correct" setting for the discriminator, possibly because of the lag introduced in the necessary smoothing process. A typical illustration is given in figure 8.

In practice, the discriminator level was set for each signal by visual observation on a dual-beam oscilloscope of simultaneous traces of the differentiated hot-wire signal and the corresponding trigger output (e. g., fig. 9). The settings of the noise clipper and of the smoothing-filter time constant were chosen by visual comparison at the beginning of the sequence of tests and kept fixed for the entire investigation.

The intermittency circuit was desgined and built by Mr. Donald S. Johnson.

VORTICITY FLUCTUATIONS

The pyramidal configuration of four hot-wires connected in a Wheatstone bridge responding primarily to the vorticity fluctuation component along the flow direction is due to Kovásznay (ref. 13). Figure 10 is an isometric sketch and a wiring diagram. Some of the pertinent details are given in reference 14.

Calibration of sensitivity to vorticity has been tried by spinning the meter about its axis (ref. 13) in a uniform flow, but for the measurements presented here an indirect method was used: The readings in a decaying isotropic turbulence were compared with the values of vorticity fluctuation level computed from turbulence level and microscale measurements. Estimates of the parasitic sensitivities, especially to the three components of turbulent velocity, were made by measuring the steady-state yaw and speed sensitivities in a low-turbulence stream. These were found to be negligibly small for the particular meter used in getting the ξ' data. No correction has been made for finite wire length (the lengths were about 1 millimeter), and no correction has been made for the nonzero ratio of wire spacing to turbulence microscale, a characteristic giving parasitic sensitivity to the second derivatives of velocity fluctuations.

MEAN VELOCITY PROFILES

A flattened no. 20 hypodermic needle was used as total-head tube in the measurement of the mean velocity profiles from which boundary-layer and jet thicknesses were determined.

Although exact wall location is probably a meaningless concept for rough-wall boundary-layer flows, the choice of such a reference value of y is convenient for presentation of data in familiar coordinates. Therefore, a $y=0$ reference was chosen by extrapolation to zero of the mean velocity profiles from a region outside the boundary tangent to the corrugation peaks. In order to minimize scatter near the "wall," all total-head traverses were made at the same phase position in the corrugation peak. A slight cutout on the downstream side in each case permitted the total-head tube to go completely into the boundary.

Since the exact details of mean velocity profile shape were not of primary concern in this investigation, no correction for the effect of turbulence has been applied to the total-head tube data.

MEASUREMENTS

MEAN VELOCITY FIELDS

Rough-wall boundary layer.—Mean velocity profiles as determined from total-head tube measurements are plotted in dimensionless form in figure 11. There is reasonably close similarity. Of course, exact similarity is not to be expected since boundary-layer Reynolds number varies considerably with x and effective roughness varies slightly.

The momentum-thickness distribution

$$\theta(x)\equiv\int_0^\infty \frac{\overline{U}}{\overline{U}_\infty}\left(1-\frac{\overline{U}}{\overline{U}_\infty}\right)dy \tag{2}$$

is given in figure 12. The solid line is a simple power law drawn from the apparent origin $x=x_o$. The similarity shown in figure 11 is close enough so that the displacement thickness

$$\delta^*(x)\equiv\int_0^\infty \left(1-\frac{\overline{U}}{\overline{U}_\infty}\right)dy \tag{3}$$

and the total thickness $\delta(x)$, the value of y at which $\overline{U}\doteq\overline{U}_\infty$, are assumed proportional to $\theta(x)$ for the purpose of later figures. The $\theta(x)$ values are assumed to be more reliable than δ^* because equation (2) deemphasizes the relatively uncertain region near the wall. The values of $\delta^*(x)$ and $\delta(x)$ are then given by $\theta(x)$ times the average values of δ^*/θ and δ/θ. These values are 1.47 and 7.2, respectively.

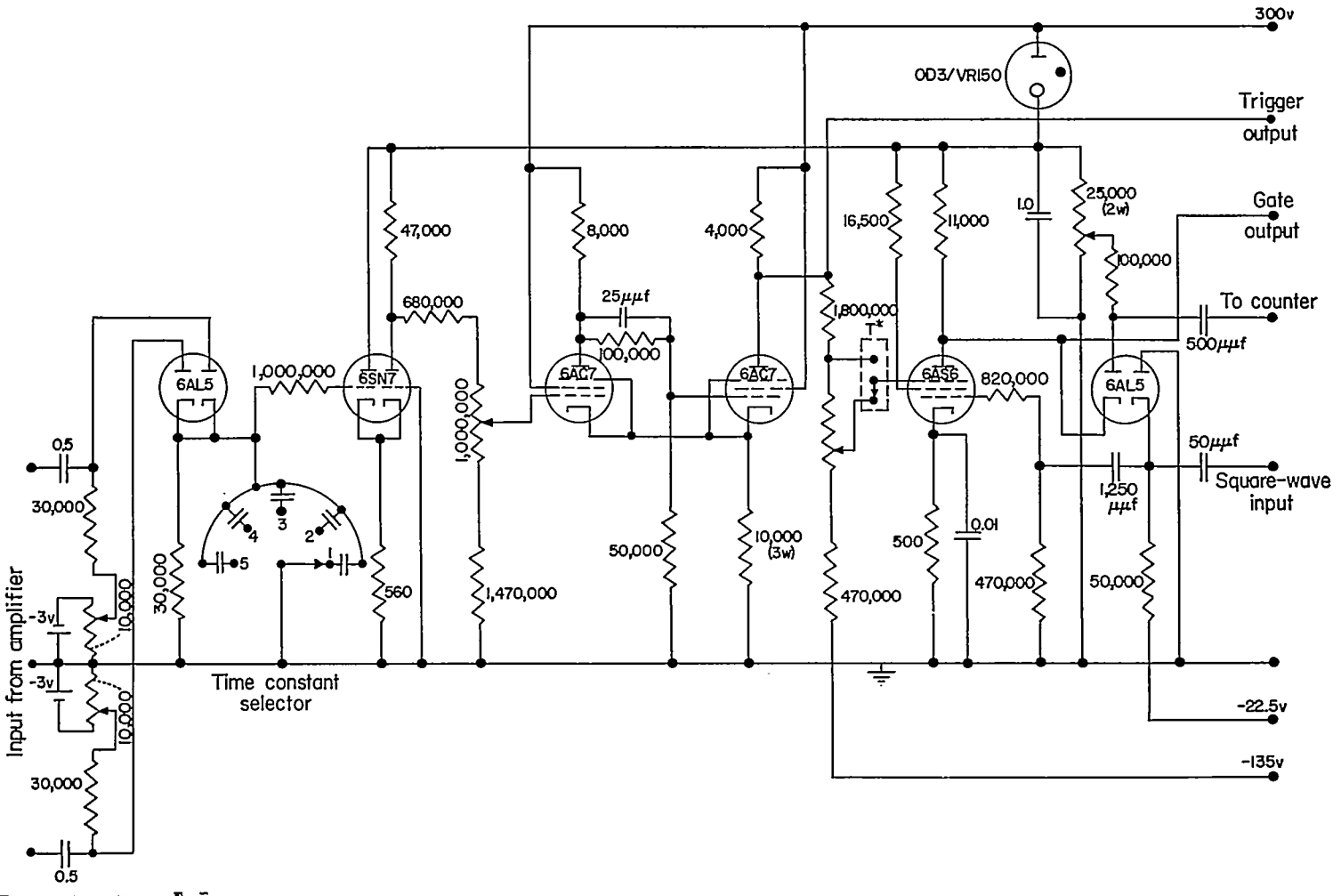

FIGURE 7.—Circuit of intermittency-measuring device. Capacitances are in microfarads unless otherwise noted; resistances, in ohms. T^*, test count rate.

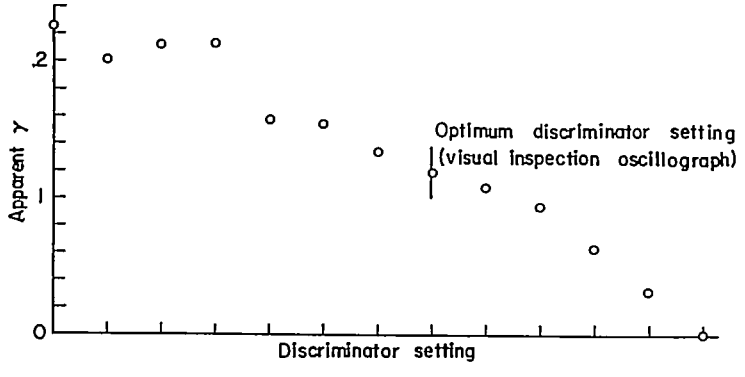

FIGURE 8.—Intermittency reading versus discriminator setting for a typical probe position.

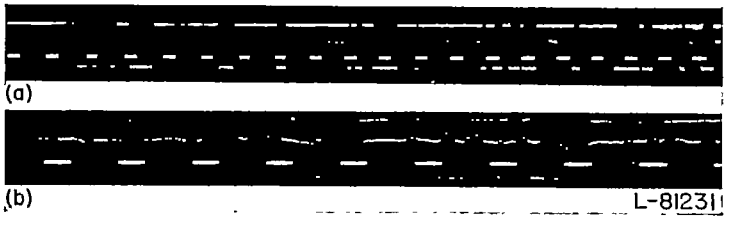

(a) Discriminator set too high (signal is $\partial u/\partial t$).
(b) Good discriminator setting (signal is $u(t)$).

FIGURE 9.—Oscillograms of hot-wire signal and trigger output.

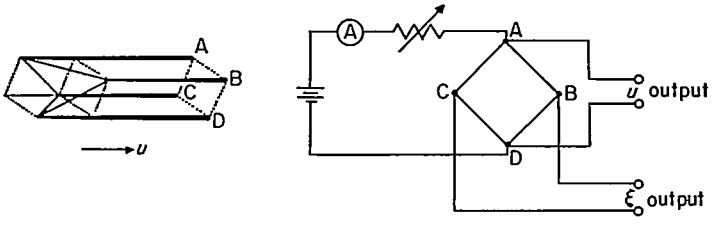

FIGURE 10.—Vorticity meter.

The skin friction coefficient

$$c_f \equiv \frac{\tau_o}{\frac{\rho}{2}\overline{U}_\infty^2} \tag{4}$$

computed from $\theta(x)$ by the Von Kármán integral relation

$$c_f = 2\frac{d\theta}{dx} \tag{5}$$

is included in figure 12.

Round jet.—Figures 13 and 14 present data for the round jet corresponding to the data for the boundary layer. The tail depression is, of course, due to the directional sensitivity of the total-head tube; at the jet edge, the mean velocity is chiefly radially inward. These measurements agree with

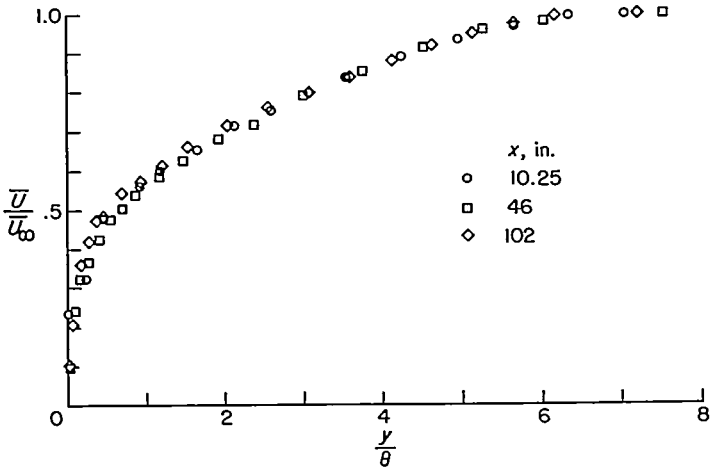

FIGURE 11.—Mean velocity profiles at several stations in rough-wall boundary layer.

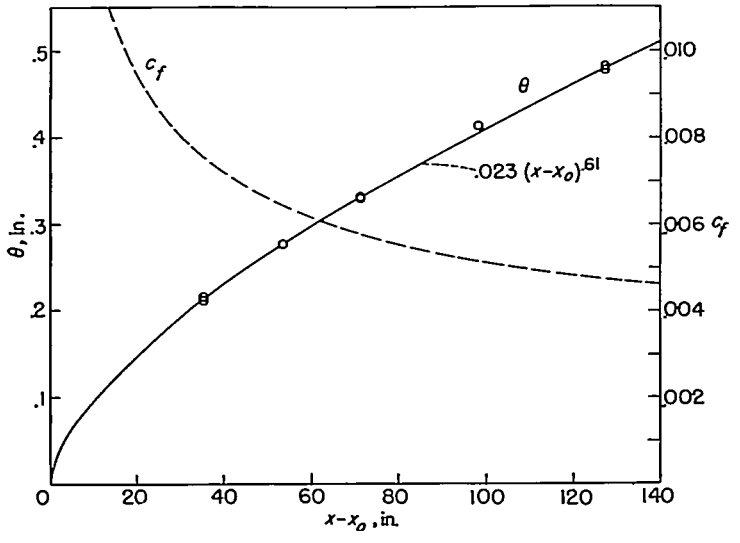

FIGURE 12.—Momentum thickness and skin friction coefficient in rough-wall boundary layer.

the results of references 2 and 12 on velocity profile and linearity of jet momentum spread with x. However, the angle of spread is slightly greater than that in reference 2, being 10.8° total angle for the half-velocity cone as against 9.5° in the earlier work

Possible factors in this difference are the following:

(a) Different orifice boundary conditions: In reference 2 the jet emerged from a plane wall about 25 orifice diameters in width; here there was no wall.

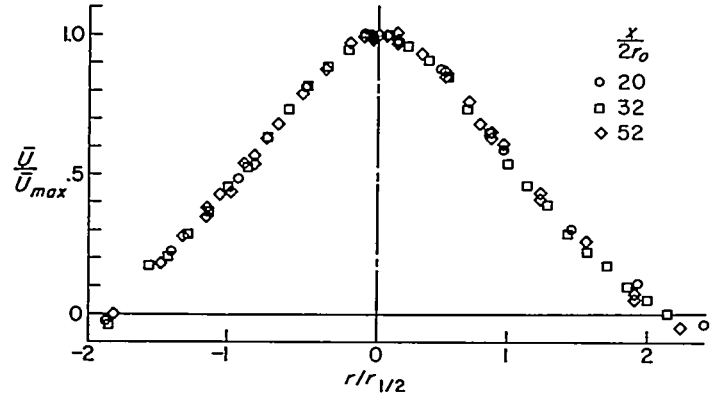

FIGURE 13.—Mean velocity profiles for round jet.

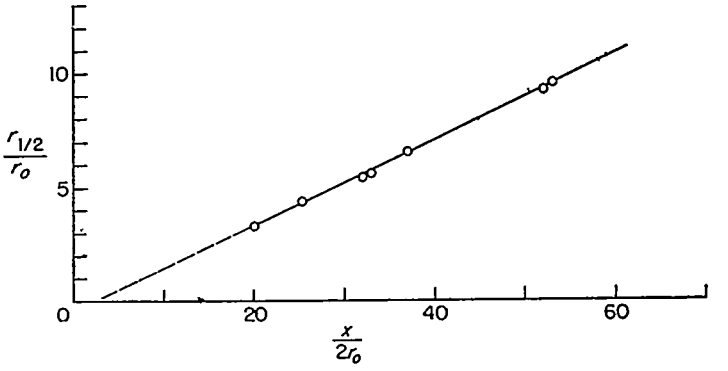

FIGURE 14.—Half-velocity radius of jet.

(b) Different Reynolds numbers: At the same x/r_o this jet field has a Reynolds number five times bigger than the one in reference 2.

(c) Different measuring instrument: The mean velocity profiles of reference 2 were measured with a hot-wire anemometer while these were measured with a total-head tube. In neither case were the data corrected for the (different) effect of turbulence on apparent mean velocity.

However, the difference is of no interest here since the principal concern is a comparison of the relative behaviors of overall mean flow field and irregular turbulence front.

CHARACTER OF FLUCTUATIONS

The intermittent character of the outer part of the turbulent boundary layer is indicated by typical oscillograms. Figure 9 includes $u(t)$ and $\partial u/\partial t$, while figure 15 includes u(t) and ξ(t). Obviously there are still appreciable velocity fluctuations in the nonturbulent parts of the flow. These are of relatively low frequency. The typical time record of vorticity fluctuations $\xi(t)$ indicates that the nonturbulent parts are irrotational, since the order of magnitude of the low-frequency fluctuations visible between turbulent segments can be accounted for by parasitic sensitivity in this particular vorticity meter.

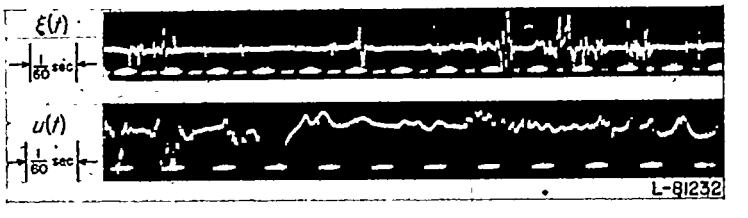

FIGURE 15.—Oscillograms of vorticity fluctuations and of longitudinal velocity fluctuations in intermittent zone.

A definite property of the $u(t)$ oscillograms is one-sidedness of the turbulent bursts. This result shows that on the average the bulges of turbulent fluid are moving more slowly than the nonturbulent fluid passing by the same lateral y-position in the boundary layer. This is not surprising, since such turbulent bulges must largely originate from further in toward the fully turbulent region, which is a region of lower mean velocity in the boundary-layer case.

This one-sidedness is sharpened up a bit by the fact that (as will be proved later) the irrotationally fluctuating fluid must be traveling at the same mean velocity as the free stream.

The qualitative description of the turbulence propagation phenomenon given in the "Introduction" requires that it actually takes place through a (presumably thin) viscous shear layer plastered all over the boundary. In fact, this "laminar superlayer" is the boundary between turbulent and nonturbulent fluid. Inspection of the oscillograms reveals no clear similarity among all the beginnings and ends of the turbulent bursts, but this is not a contradiction of the physical picture. Any such tendency must be completely masked by the randomness of velocity gradients (and hence the shears) in the laminar superlayer. Furthermore, the boundary itself is an irregularly wrinkled surface in three dimensions so that the relative orientations of hot-wire and boundary at the moments of immersion and withdrawal are also random.

TURBULENCE LEVELS

Turbulence-level distributions for the three velocity components $u'/\overline{U}$, $v'/\overline{U}$, and $w'/\overline{U}$ at the boundary-layer station studied in detail ($x=102$ inches) are plotted in figure 16, with the corresponding mean velocity profile included for reference. Clearly the velocity fluctuations due to the presence of the boundary layer extend far outside the region conventionally identified as the boundary layer.

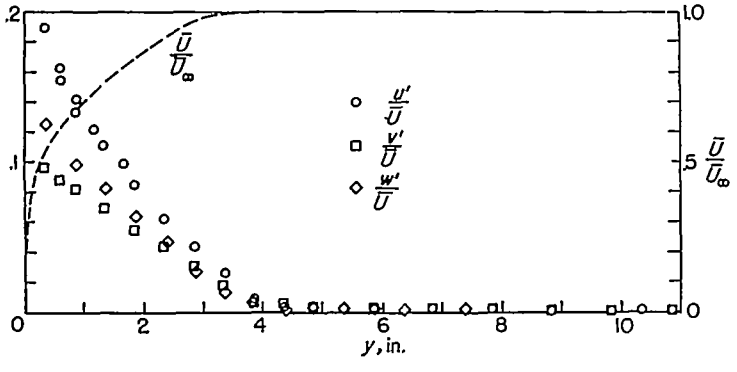

FIGURE 16.—Turbulence-level distributions at $x=102$ inches in boundary layer.

Variation of turbulence level in the x-direction, for corresponding locations in the boundary layer, is indicated by $v'/\overline{U}$ versus x at several fixed values of y/δ (fig. 17). Since the Prandtl friction velocity $U_\tau \equiv \sqrt{\frac{\tau_0}{\rho}}$ is probably the basic reference quantity with the dimensions of Length/Time in a solid-wall shear flow, one expects that, for corresponding positions in the boundary layer, u', v', and $w' \propto U_\tau$. In turbulent pipe flow, Laufer (ref. 15) finds that v'/U_τ versus radius is independent of Reynolds number except in the vicinity of the wall. This suggests that, in the boundary layer, v'/U_τ versus y/δ may be constant away from the wall. Figure 17 shows at least no clear-cut contradiction with this hypothesis, within the overall experimental uncertainty.

TURBULENT SHEAR STRESS

The turbulent shear stress distribution $-\rho\overline{uv}(y)$, at $x=102$ inches, is presented in dimensionless form in figure 18 and shows the same behavior as in the smooth-wall cases (refs. 4 and 16), approaching zero appreciably faster than

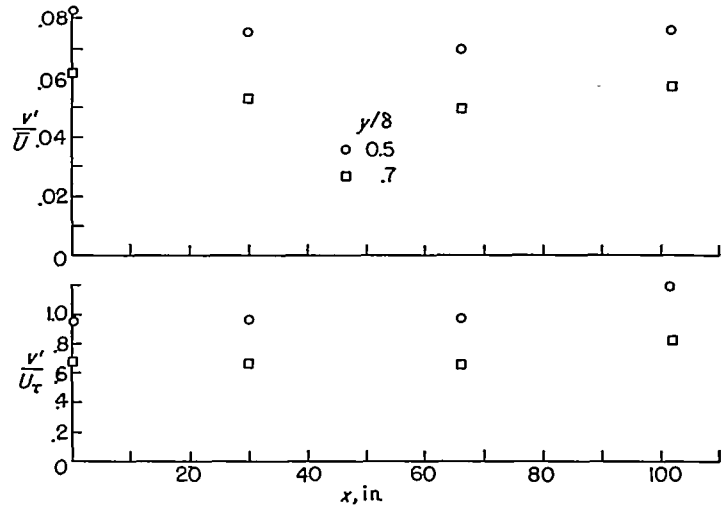

FIGURE 17.—Boundary-layer turbulence level as a function of x for corresponding y-positions

the squared fluctuation intensities $(u')^2$, $(v')^2$, and $(w')^2$. The shear correlation coefficient $R_{uv}=\overline{uv}/u'v'$ becomes quite uncertain in the outer part of the boundary layer because the measurement then involves the taking of small differences between relatively large uncertain readings.

VORTICITY FLUCTUATION LEVEL

The measured distribution of root-mean-square vorticity fluctuation (ξ', the x-component only) across the boundary layer at $x=102$ inches is given in figure 18. The instrument was by chance sufficiently symmetrical that, within the purposes of this investigation, no correction for parasitic sensitivities was necessary.

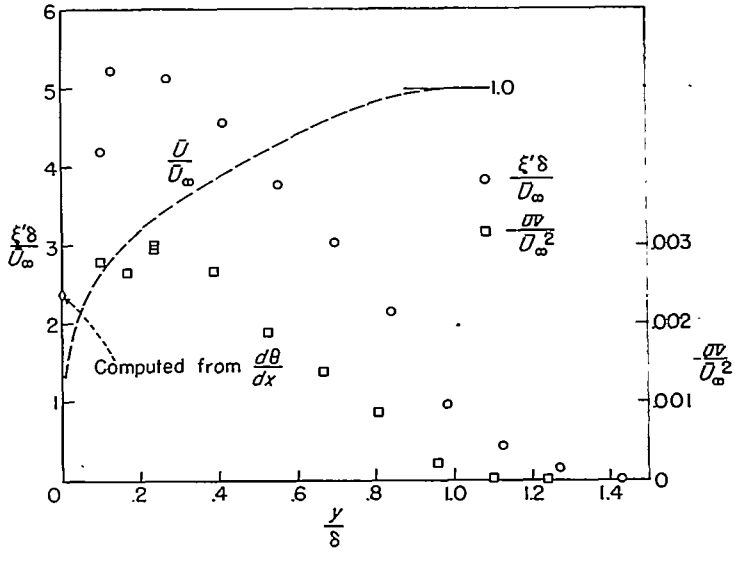

FIGURE 18.—Vorticity fluctuation and turbulent shear-stress distributions in boundary layer at $x=102$ inches.

INTERMITTENCY

Boundary layer.—The transversal distributions of intermittency $\gamma(y)$ at several x-stations in the boundary layer (typical comparison with $\overline{U}/\overline{U}_\infty$ in fig. 19) show good similarity when y is normalized with $\sigma(x)$, the square root of the second moment of $\partial\gamma/\partial y$ with y-origin chosen so that $\partial\gamma/\partial y$ has zero first moment (fig. 20). As pointed out in the "In-

troduction," $\partial\gamma/\partial y$ is the probability density of $Y(t)$, the instantaneous y-position of the front between turbulent and nonturbulent fluid, at a fixed x. Then

$$\sigma(x)=\left[\overline{(Y-\overline{Y})^2}\right]^{1/2}=\left[\int_{-\infty}^{\infty}(y-\overline{Y})^2\frac{\partial\gamma}{\partial y}d(y-\overline{Y})\right]^{1/2} \quad (6)$$

where $\partial\gamma/\partial y$ is written as a function of $(y-\overline{Y})$. Therefore, $\sigma(x)$ is a suitable measure of the width of the intermittent zone, that is, of the wrinkle amplitude of the turbulence front.

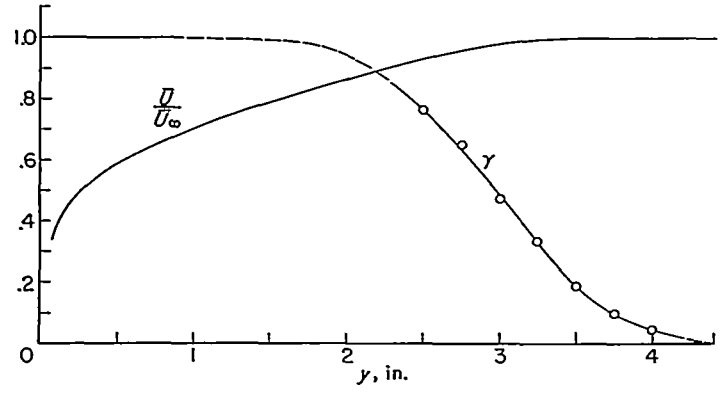

FIGURE 19.—Typical intermittency distribution across boundary layer.

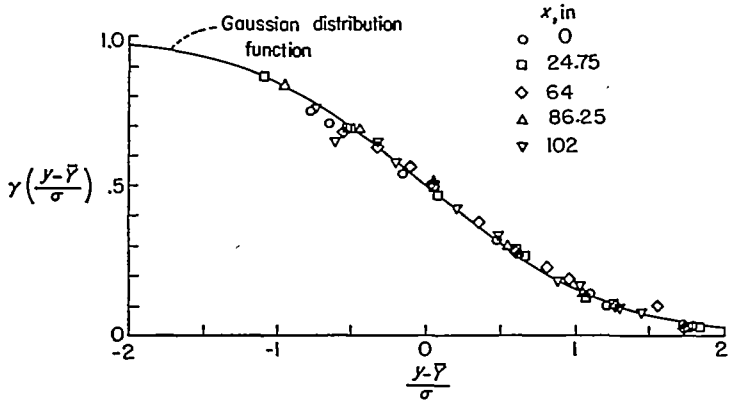

FIGURE 20.—Intermittency distributions for several x-stations in boundary layer.

Another important statistical measure of the turbulence front is its average location,

$$\overline{Y}(x)=\int_{-\infty}^{\infty}y\frac{\partial\gamma}{\partial y}dy \quad (7)$$

Since $\partial\gamma/\partial y$ turned out to be symmetrical and, in fact, virtually Gaussian within the experimental precision (see section "Probability Density of $Y(t)$"), the determination of σ and $\overline{Y}$ was considerably simplified. Both $\sigma(x)$ and $\overline{Y}(x)$ are given in figure 21 and $\delta(x)$ is included for comparison. The logarithmic plot was used to estimate exponents in power-law approximations for the three quantities.

The power-law fitting has been done with the best common origin for the three sets of points in order to simplify the comparison concept.

Round jet.—Intermittency data for the round jet corresponding to the data for the boundary layer are given in figures 22, 23, and 24.

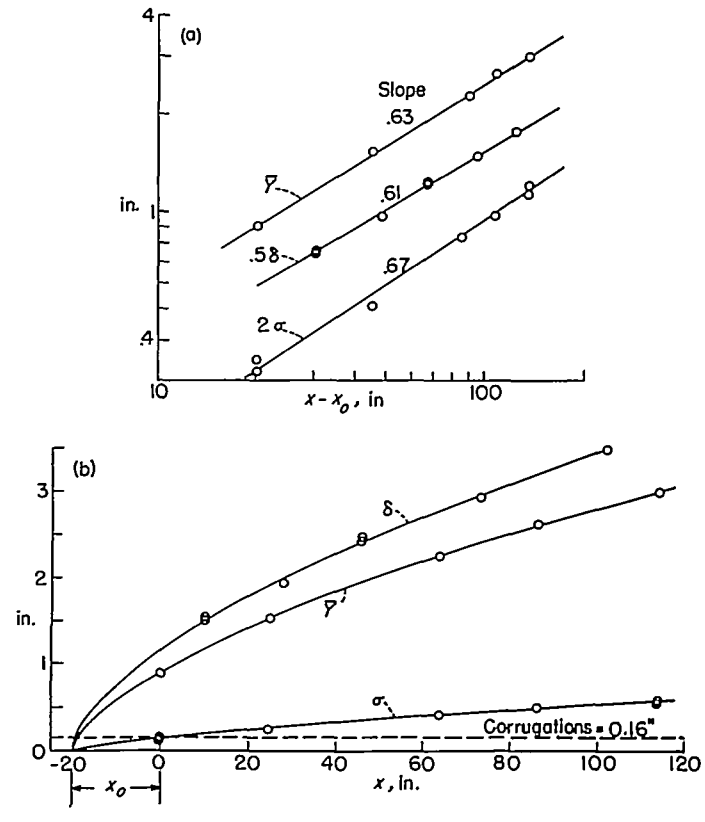

(a) Function of $x-x_o$.
(b) Function of x.

FIGURE 21.—Amplitude and average position of turbulence front in boundary layer as functions of x and $x-x_o$.

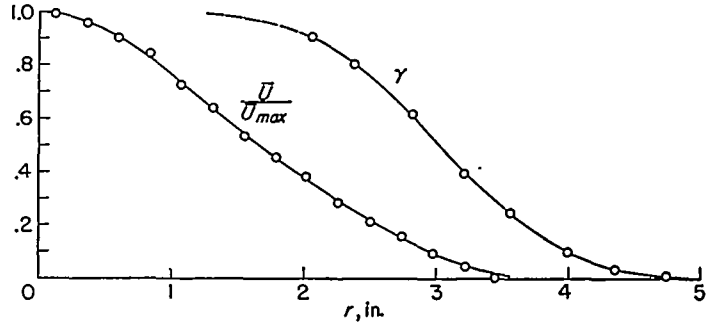

FIGURE 22.—Typical intermittency distribution across round jet.

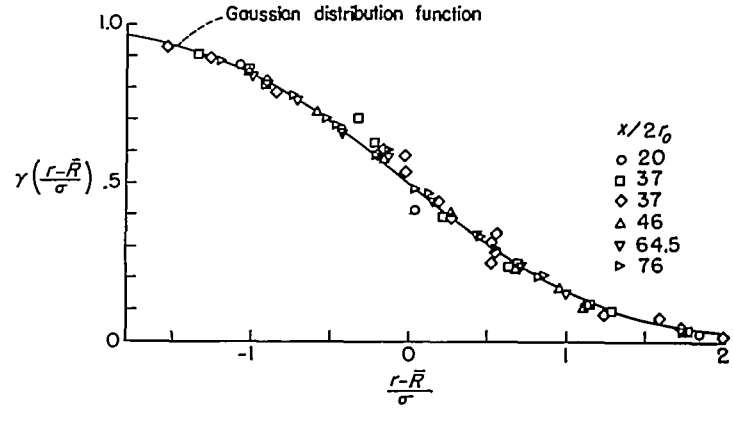

FIGURE 23.—Intermittency distributions for several x-stations in round jet.

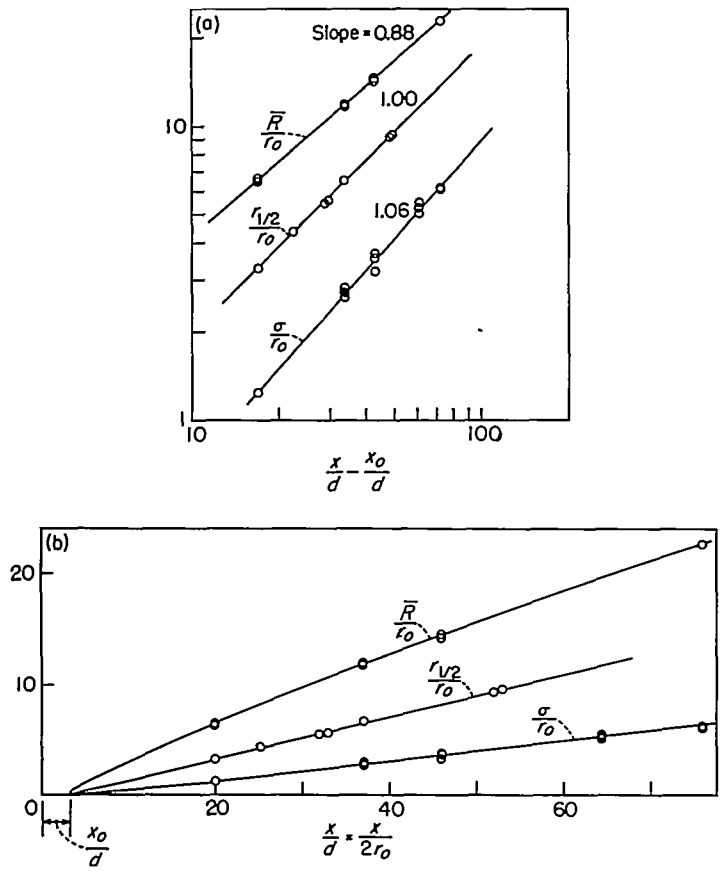

(a) Amplitude of turbulence front.
(b) Average position of turbulence front.

FIGURE 24.—Amplitude and average position of turbulence front in round jet as functions of $x/2r_o$.

Townsend's plane wake.—For convenient comparison Townsend's last published data (ref. 10) for the plane wake have been put into a form corresponding to that of the other data (figs. 25, 26, and 27).

Since, however, only the points for $x/d = 800$ and 950 are in the fully developed wake, no attempt has been made to determine separate power laws from his data. Instead,

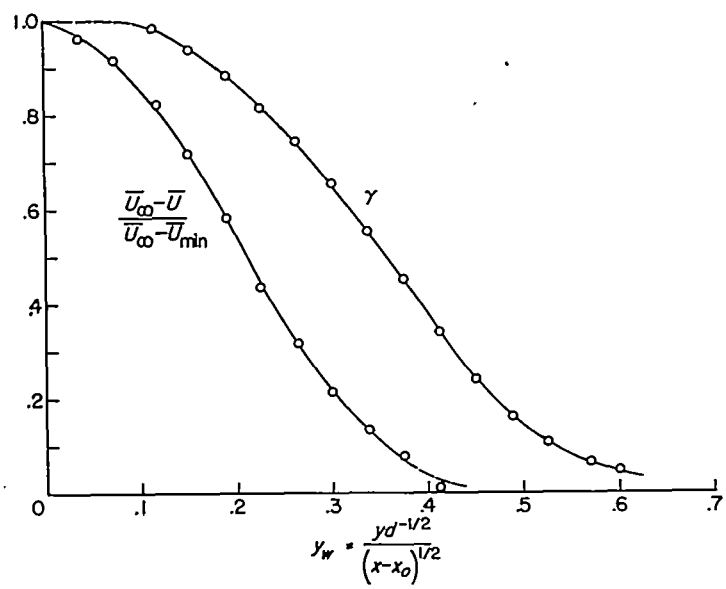

FIGURE 25.—Typical intermittency distribution across a plane wake. (Data from ref. 10.)

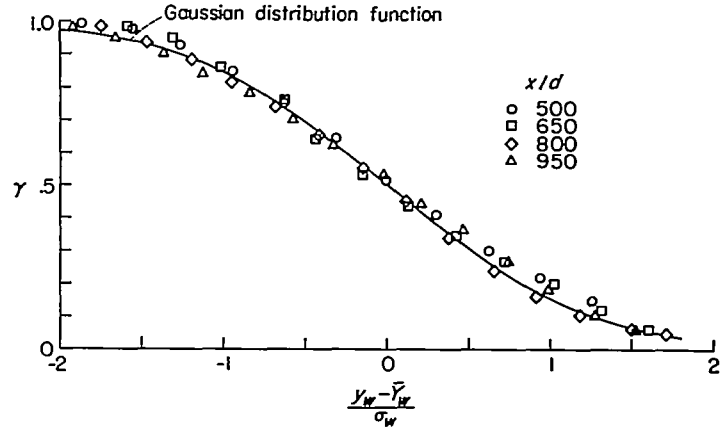

FIGURE 26.—Intermittency distributions for several x-stations in plane wake. (Data from ref. 10.)

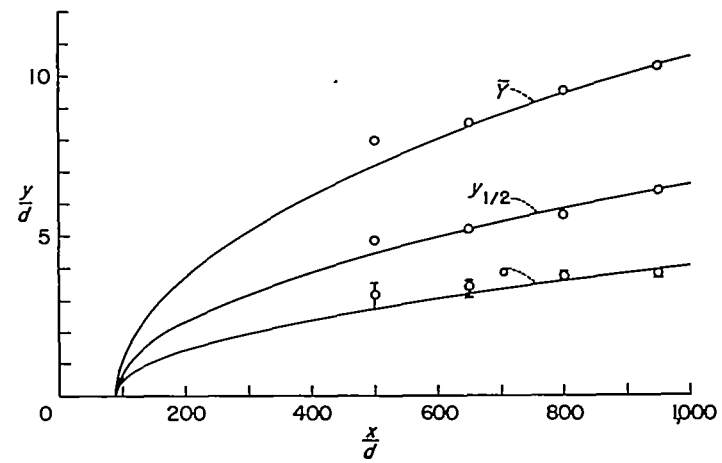

FIGURE 27.—Amplitude and average position of turbulence front in plane wake as functions of x. (Data from ref. 10.)

parabolas have been drawn with his choice of apparent origin simply to show that his results are not in contradiction with the parabolic $\sigma(x)$ and $\overline{Y}(x)$ (predicted theoretically in a later section).

STATISTICAL ANALYSIS OF ON-OFF INTERMITTENCY SIGNAL

(Output of Schmitt Trigger)

As sketched in figure 6, one stage in the electrical signal manipulation sequence is a two-valued (on-off) random function. These flat-top pulses have duration equal to the time spent by the hot-wire in turbulent fluid and spacing equal to the time spent in nonturbulent fluid.

Two basic statistical characteristics of such a random on-off signal are (a) its power spectrum and (b) the probability densities of its top lengths and its bottom lengths. Except in special cases, no one has yet deduced a relation between these two functions (see section "Probability Density of Pulse Lengths").

Since the jumps in this signal are generated by the random occurrence of a particular amplitude of a more general stationary random variable, that is, $Y(t)$, its properties give some information on the properties of $Y(t)$. For example, the probability densities of top and bottom lengths indicate the statistical distribution of wave lengths of the turbulence front, though less directly than the way in which $\partial\gamma/\partial y$ gives the statistical distribution of amplitudes. A detailed dis-

cussion follows in the section "Statistical Description of Turbulence Front."

The power spectrum of the on-off signal must be related to that of the total hot-wire signal, though not in any simple fashion. As will be pointed out later, considering the total signal as continuous turbulence modulated by this on-off signal, it appears that carrier and modulation must be statistically independent for the power spectra to combine simply.

Figure 28 is a series of power spectra $F_c(n)$ of the Schmitt trigger output at various values of γ for $x=102$ inches. Statistical symmetry of $\Upsilon(t)$ (indicated by the approximate symmetry of $\partial\gamma/\partial y$) requires that $F_c(n)$ for intermittency $\gamma=\gamma_1$ be equal to $F_c(n)$ for intermittency $\gamma=1-\gamma_1$. Figure 29 gives the probability densities of tops and of bottoms at the same hot-wire locations. These were obtained by direct measurement of oscillographic records.

The solid line in figure 28 is the theoretical power spectrum for a random flat-top signal whose jumps have a Poisson distribution in time (see section "Power Spectrum of Schmitt Trigger Output," especially eq. (88)).

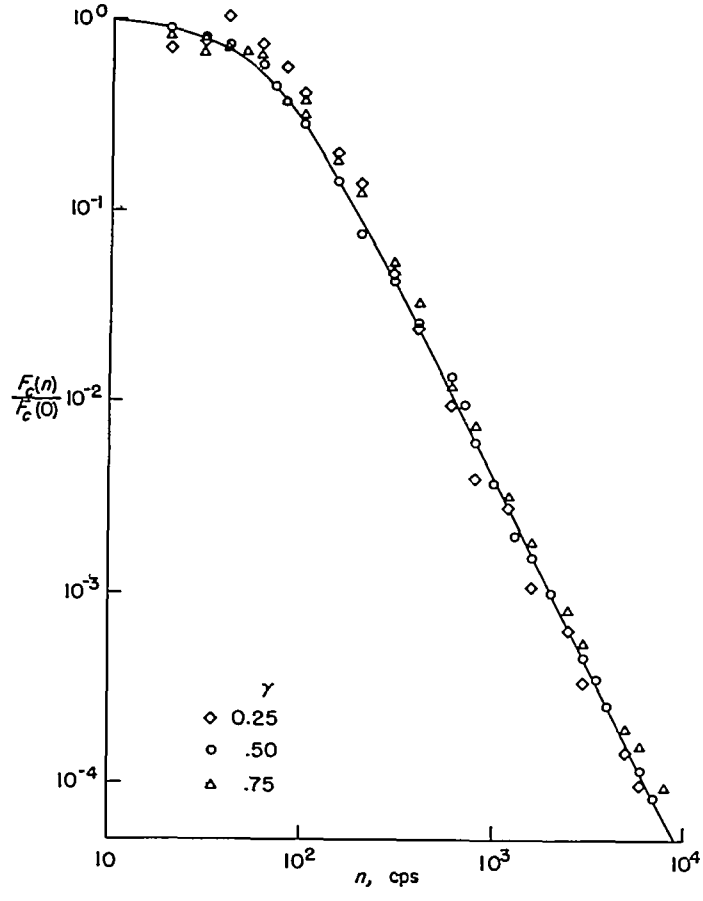

FIGURE 28.—Power spectra of Schmitt trigger outputs for three different intermittencies in boundary layer at $x=102$ inches.

$$\frac{F_c(n)}{F_c(0)}=\frac{1}{1+2.49\times10^{-4}n^2}$$

THEORETICAL EXISTENCE OF TURBULENCE FRONT

Although the relatively sharp front between turbulent and nonturbulent fluid has been well established experimentally, this apparently ubiquitous phenomenon must still be explained and explored analytically. The oscillographic

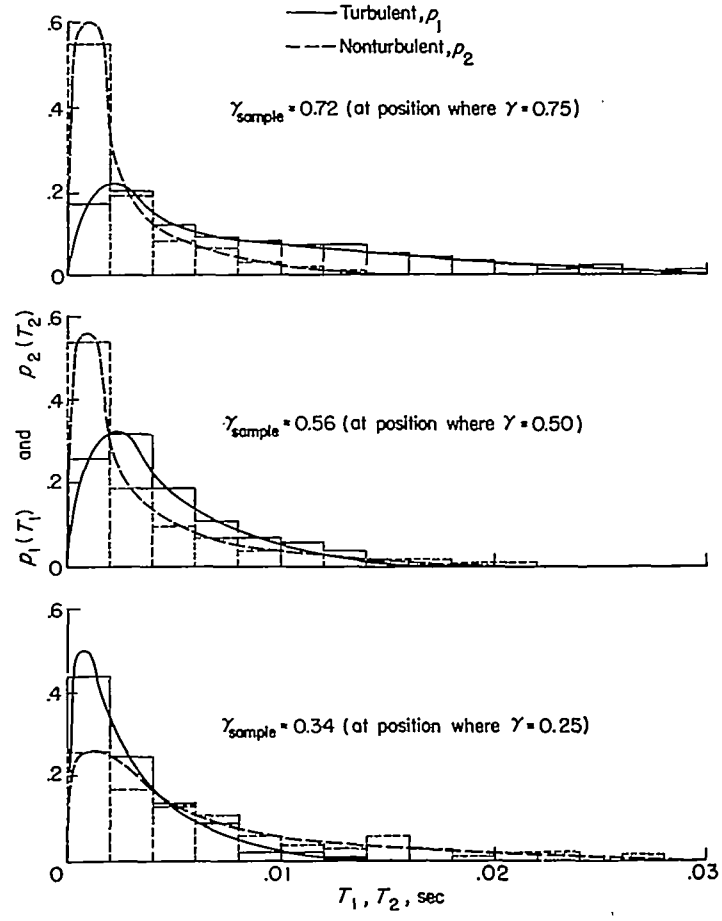

FIGURE 29.—Probability densities of segment lengths of intermittent signal for three different intermittencies in boundary layer at $x=102$ inches.

records indicate that it is likely to be a boundary between rotational and irrotational motion. The theoretical discussion will therefore aim first at heuristic demonstration of this concept by showing in this context the known fact that turbulent stretching of the vortex lines in a local vorticity gradient tends to steepen the gradient (leading, of course, in the limit to zero vorticity on one side).

Succeeding sections will discuss some of the ramifications of this physical picture, in preparation for the more detailed analyses which follow. The degree of agreement between the predictions of these analyses and actual experimental results will provide further indication of the validity of the hypothesis that the nonturbulent field is actually irrotational.

STEEPENING OF A VORTICITY GRADIENT WITH LOCAL PRODUCTION OF VORTICITY

Since the distinction to be made here between turbulent and nonturbulent flow is on the basis of presence or absence, respectively, of random vorticity fluctuations, the boundary phenomena must obviously be studied in terms of vorticity as a principal characteristic variable.

The vector form of the vorticity equation for three-dimensional incompressible viscous flow is

$$\frac{D\underline{\Omega}}{Dt}=(\underline{\Omega}\cdot\nabla)\underline{Q}+\nu\nabla^2\underline{\Omega} \tag{8}$$

where $\frac{D}{Dt}\equiv\left(\frac{\partial}{\partial t}+\underline{Q}\cdot\nabla\right)$ is the Stokes derivative (following a fluid element), $\underline{\Omega}$ is total vorticity vector, $\underline{Q}$ is total velocity vector and ν is kinematic viscosity.

Introducing a Reynolds type restriction:

$$\underline{\Omega}(\underline{r},t)=\overline{\underline{\Omega}}(\underline{r})+\underline{\omega}(\underline{r},t) \qquad \overline{\underline{\omega}}\equiv 0$$

$$\underline{Q}(\underline{r},t)=\overline{\underline{Q}}(\underline{r})+\underline{q}(\underline{r},t) \qquad \overline{\underline{q}}\equiv 0$$

equation (8) yields the mean-vorticity equation:

$$(\overline{\underline{Q}}\cdot\nabla)\overline{\underline{\Omega}}+\overline{(\underline{q}\cdot\nabla)\underline{\omega}}=(\overline{\underline{\Omega}}\cdot\nabla)\overline{\underline{Q}}+\overline{(\underline{\omega}\cdot\nabla)\underline{q}}+\nu\nabla^2\overline{\underline{\Omega}} \tag{9}$$

Subtracting equation (9) from equation (8) leaves the equation for vorticity fluctuation:

$$\frac{\partial\underline{\omega}}{\partial t}+(\underline{q}\cdot\nabla)\overline{\underline{\Omega}}+(\overline{\underline{Q}}\cdot\nabla)\underline{\omega}+(\underline{q}\cdot\nabla)\underline{\omega}-\overline{(\underline{q}\cdot\nabla)\underline{\omega}}=$$

$$(\underline{\Omega}\cdot\nabla)\underline{q}+(\underline{\omega}\cdot\nabla)\overline{\underline{Q}}+(\underline{\omega}\cdot\nabla)\underline{q}-\overline{(\underline{\omega}\cdot\nabla)\underline{q}}+\nu\nabla^2\omega \tag{10}$$

The scalar product of $\underline{\omega}$ with equation (10) gives the equation for instantaneous vorticity intensity:

$$\frac{1}{2}\frac{D\omega^2}{Dt}+\underline{\omega}\cdot[(\underline{q}\cdot\nabla)\overline{\underline{\Omega}}]-\underline{\omega}\cdot\overline{[(\underline{q}\cdot\nabla)\underline{\omega}]}=\underline{\omega}\cdot[(\overline{\underline{\Omega}}\cdot\nabla)\underline{q}]+$$

$$\underline{\omega}\cdot[(\underline{\omega}\cdot\nabla)\overline{\underline{Q}}]+\underline{\omega}\cdot[(\omega\cdot\Delta)\underline{q}]-\underline{\omega}\cdot\overline{[(\underline{\omega}\cdot\nabla)\underline{q}]}+\nu\underline{\omega}\cdot(\nabla^2\underline{\omega}) \tag{11}$$

In Cartesian tensor notation, but keeping vorticity as a vector instead of an antisymmetric second-rank tensor,

$$\frac{1}{2}\frac{D\omega^2}{Dt}+\xi_i u_j\frac{\partial\overline{\Xi}_i}{\partial x_j}-\xi_i\left(\overline{u_j\frac{\partial\xi_i}{\partial x_j}}\right)=\xi_i\overline{\Xi}_j\frac{\partial u_i}{\partial x_j}+\xi_i\xi_j\frac{\partial\overline{U}_i}{\partial x_j}+$$

$$\xi_i\xi_j\frac{\partial u_i}{\partial x_j}-\xi_i\left(\overline{\xi_j\frac{\partial u_i}{\partial x_j}}\right)+\nu\xi_i\nabla^2\xi_i \tag{11a}$$

where a repeated index indicates summation and $\omega^2=\xi_i\xi_i$.

The averaged equation is

$$\frac{1}{2}\overline{U}_j\frac{\partial\overline{\omega^2}}{\partial x_j}+\frac{1}{2}\frac{\partial}{\partial x_j}(\overline{u_j\omega^2})+\overline{\xi_i u_j}\frac{\partial\overline{\Xi}_i}{\partial x_j}=\overline{\Xi}_j\overline{\xi_i\frac{\partial u_i}{\partial x_j}}+$$

$$\overline{\xi_i\xi_j}\frac{\partial\overline{U}_i}{\partial x_j}+\overline{\xi_i\xi_j\frac{\partial u_i}{\partial x_j}}+\nu\overline{\xi_i\nabla^2\xi_i} \tag{12}$$

It was Taylor (ref. 17) who first identified $\overline{\xi_i\xi_j\frac{\partial u_i}{\partial x_j}}$ as the rate of production of vorticity fluctuations by the random stretching of vortex lines. It is largely the absence of this effect that makes fully two dimensional motion trivial in the problem of fully developed turbulence.

To demonstrate the tendency of a vorticity gradient to steepen in the presence of this vorticity production effect, consider the simplified form of equation (11a) for a flow with no mean velocity or vorticity:

$$\frac{1}{2}\frac{\partial\omega^2}{\partial t}+\frac{1}{2}u_j\frac{\partial\omega^2}{\partial x_j}-\xi_i\left(\overline{u_j\frac{\partial\xi_i}{\partial x_j}}\right)=$$

$$\xi_i\xi_j\frac{\partial u_i}{\partial x_j}-\xi_i\left(\overline{\xi_j\frac{\partial u_i}{\partial x_j}}\right)+\nu\xi_i\nabla^2\xi_i \tag{13}$$

It appears that no conclusion can be reached without further restriction. Since the vorticity spectrum varies like $k^2F(k)$, the running second moment of the velocity spectrum, vorticity-dominated phenomena must be associated with the fine structure of the turbulence, especially for high values of turbulence Reynolds number $R_\lambda\equiv u'\lambda/\nu$, where u' is root-mean-square velocity fluctuation in the x-direction and λ is the Eulerian microscale. For large enough values of R_λ there should exist a time long compared with that characterizing the main body of vorticity fluctuations but short compared with that characterizing the largest scale velocity fluctuations, which dominate the convective properties of the turbulence. For example, one can expect

$$\frac{1}{\xi'\lambda_t}\ll 1 \tag{14}$$

where ξ' is the root-mean-square x-component of vorticity fluctuation and λ_t is the Lagrangian time microscale (ref. 1). Introducing $\lambda_\eta\equiv v'\lambda_t$ (ref. 18) and, with local isotropy, the isotropic relation $\xi'=\sqrt{5}\frac{v'}{\lambda}$, equation (14) becomes

$$0.45\left(\frac{\lambda}{\lambda_\eta}\right)\ll 1 \tag{15}$$

or, in terms of R_λ, the large R_λ approximation for λ/λ_η gives (ref. 18)

$$\frac{2.4}{\sqrt{R_\lambda}}\ll 1 \tag{16}$$

For flows with equation (16) valid, equation (13) could be averaged over a time long enough to average vorticity phenomena but short for convective velocity phenomena:

$$\frac{1}{2}\frac{\partial\overline{\overline{\omega^2}}}{\partial t}+\frac{1}{2}u_j\frac{\partial\overline{\overline{\omega^2}}}{\partial x_j}\approx\overline{\overline{\xi_i\xi_j}}\frac{\partial\overline{u_i}}{\partial x_j}+\overline{\overline{\nu\xi_i\nabla^2\xi_i}} \tag{17}$$

where $\overline{\overline{(\ )}}\approx\overline{(\ )}$ for the fine-structure variables.

The velocity derivative has characteristic time like that of vorticity.

Since the objective is to show the steepening of the $\overline{\overline{\omega^2}}$ gradient in the absence of ν, omit the last term and write

$$\frac{1}{2}\frac{D\overline{\overline{\omega^2}}}{Dt}\approx\overline{\overline{\xi_i\xi_j}}\frac{\partial\overline{u_i}}{\partial x_j} \tag{18}$$

Therefore,

$$\frac{1}{2}\frac{D}{Dt}\left(\frac{\partial\overline{\overline{\omega^2}}}{\partial y}\right)\approx\frac{\partial}{\partial y}\left(\overline{\overline{\xi_i\xi_j}}\frac{\partial\overline{u_i}}{\partial x_j}\right) \tag{19}$$

Taylor (ref. 17) has shown that $\overline{\xi_i\xi_j\frac{\partial u_i}{\partial x_j}}>0$ for isotropic turbulence. In fact, since this inequality just expresses the general tendency for fluid lines to lengthen in a turbulent flow, it seems clear that $\overline{\overline{\xi_i\xi_j}}\frac{\partial\overline{u_i}}{\partial x_j}>0$ in any turbulence. Then, if $\overline{\overline{\xi_i\xi_j}}\frac{\partial\overline{u_i}}{\partial x_j}$ is monotonic with $\overline{\overline{\omega^2}}$, it follows from equation (19) that $\frac{D}{Dt}\left(\frac{\partial\overline{\overline{\omega^2}}}{\partial y}\right)$ has the same sign as $\partial\overline{\overline{\omega^2}}/\partial y$, which means a steepening of this $\overline{\overline{\omega^2}}$ gradient.

The physical reason for the steepening tendency is, of course, just the fact that the rate of production of new vorticity by line stretching is proportional to the vorticity already present at any point in the fluid. Hence the higher vorticity regions experience a greater rate of increase of vorticity than the lower vorticity regions, that is, the gradients tend to steepen up, limited finally by viscous diffusion and dissipation. Of course, the gradient of concern here is that in the zone between fully turbulent fluid and nonturbulent fluid. A steepening of this gradient means a tendency toward a relatively sharp surface of demarcation between the two states. The above discussion does not treat the question of the equilibrium thickness ϵ of the laminar superlayer that results; this will be estimated later. Of course, for the turbulence front to be sharp as observed experimentally, it must be shown that $\epsilon \ll \delta$.

Although the analysis is valid only for extremely high values of R_λ, far higher, in fact, than those that occur in the experiments reported here, there appears to be no reason for the situation to change qualitatively at lower values of R_λ, as long as nonlinear effects in the Navier-Stokes equations remain important, for example, $R_\lambda > 10$.

LAMINAR SUPERLAYER

Vorticity can be transmitted to an irrotational flow only through the tangential forces due to viscosity; it cannot be transmitted to the irrotational flow by macroscopic Reynolds type shear forces. It therefore follows that the instantaneous border zone lying between turbulent fluid and irrotational fluid must be a region in which viscous forces play a central role, in spite of the presence of velocity fluctuations which dominate the gross momentum transfer of the turbulent field. This border zone may be termed the laminar superlayer and is exactly what is also referred to in this report as the turbulence front, although the latter designation implies emphasis on its overall behavior rather than its detailed structure.

This laminar superlayer differs in function from the well-known laminar sublayer at the smooth solid boundary of a channel, pipe, or boundary-layer flow. The sublayer is a relatively fixed region in which mean flow momentum is transported primarily by a net mean viscous (laminar) shear force. It transmits little mean vorticity (being a zone of roughly constant $\overline{\Omega}(y)$) and it remains "attached" more or less to the same fluid particles. On the other hand, the superlayer is a (convectively) randomly moving layer of fluid which probably transports relatively small amounts of mean momentum and vorticity by viscous shear forces; its distinguishing function is transport of vorticity fluctuations and mean vorticity, when present, into what was previously an irrotational field, and in so doing it continuously propagates (relatively to local fluid) normal to its local "plane."

Sketches (a) and (b) illustrate the concept of the superlayer as a very narrow zone in which the vorticity fluctuation level and the total shear (if any) drop from values characteristic of fully turbulent flow to practically zero.

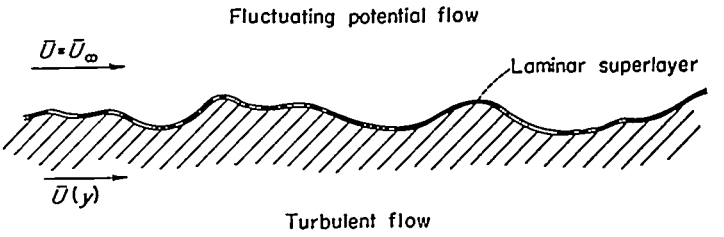

Sketch (a).

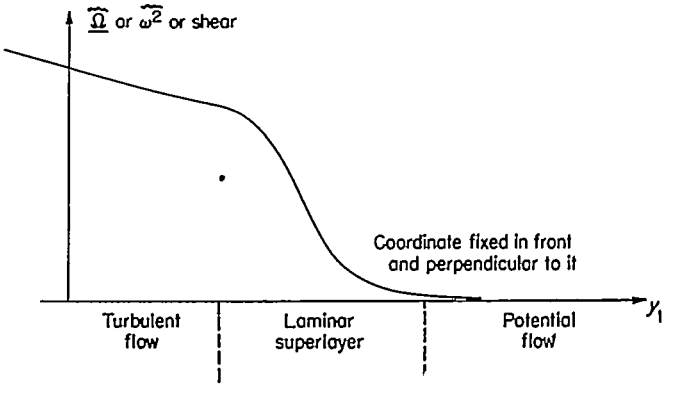

Sketch (b).

While the instantaneous local viscous shear force in a laminar sublayer is predominantly in the direction of the mean shear force, that in the superlayer must have a much higher fluctuation level, often reversing its direction, for example. In fact, in a flow field with constant mean velocity everywhere, the superlayer viscous shear force would have no mean value at all.

The discussion headed "Steepening of a Vorticity Gradient With Local Production of Vorticity" is a justification (not a proof) of the experimental fact that the continuous fluid-line stretching due to the velocity fluctuations tends to steepen up the laminar superlayer. This steepening effect is reinforced by the propagation and must, of course, be balanced out at some state by the diffusive action of viscosity, so that the superlayer must have some average thickness. From the oscillograms, it appears that this quantity, ϵ say, is very small.

Some heuristic comments can be made about this thickness. First of all, since the layer is primarily a vorticity-propagating device, its thickness should be less than a length characterizing vorticity fluctuations on the turbulent side of the boundary, for example, the dissipation scale λ (Taylor's microscale). In fact, as a characteristic viscous shear length, it might be expected to be the same order as Kolmogoroff's minimum length $\left(\frac{\nu^3}{\Phi}\right)^{1/4}$, where Φ is the rate of dissipation of turbulent energy per unit mass of fluid.

A second intuitive specification is that, as a violently disturbed free laminar shear layer, its characteristic Reynolds number should be on the order of the lower critical Reynolds number for free laminar shear layers. A possible choice of characteristic instantaneous Reynolds number would be that based on thickness and instantaneous tangential velocity difference Δ across the superlayer. When the

instantaneous viscous shear force, $\underline{S} \approx \mu \frac{\underline{\Delta}}{\epsilon}$ per unit area in the plane of the front, has a nonzero average (i. e., a preferred direction), a plausible average Reynolds number might be

$$ {}_1R_\epsilon \equiv \frac{\Delta\, \overline{\epsilon}}{\nu} \tag{20} $$

where Δ is the magnitude of $\underline{\Delta}$. Of course, Δ and ϵ are doubtless negatively correlated, but inclusion of such a refinement would be inconsistent with the crude nature of the discussion.

For turbulence fronts in which there is little or no mean velocity difference across the superlayer, the above definition is inapplicable and might be replaced by

$$ {}_2R_\epsilon \equiv \frac{\Delta' \overline{\epsilon}}{\nu} \tag{21} $$

again omitting the implications of $\Delta\epsilon$ correlation.

Since, however, there still exists no analysis relating $\underline{\Delta}$ to the properties of the turbulence, a third definition, replacing ${}_{1,2}R_\epsilon$ and including such properties, is preferable:

$$ R_\epsilon \equiv \frac{\omega' \overline{\epsilon}^2}{\nu} \tag{22} $$

In fact, this definition is not too different from the other two: Δ/ϵ must be of the same order as the neighboring turbulent vorticity fluctuations.

Given an order of magnitude of the lower critical Reynolds number for free laminar shear flow plus a measurement or estimate of $\omega' = \sqrt{\overline{\xi^2} + \overline{\eta^2} + \overline{\zeta^2}}$ in the turbulence near the front, an estimate can be made for $\overline{\epsilon}$.

The only information available for estimating the desired Reynolds number is the partial analysis of Lessen (ref. 19), a small-perturbation analysis. Extrapolation of his neutral stability curve (a highly inaccurate process) suggests an estimate

$$ 1 < R_\epsilon < 10 $$

The measured turbulent value of ξ' for a typical case (fig. 18) is about 400 per second, which gives $\omega' \approx 700$ per second, if there is approximately local isotropy. With $\nu = 0.15$ square centimeter per second the estimate of superlayer thickness turns out to be

$$ 0.015 < \overline{\epsilon} < 0.05 \text{ centimeters} $$

This appears to be a reasonable order of magnitude since $\lambda \approx 0.2$ centimeter in this part of the flow. The Kolmogoroff length $\left(\frac{\nu^3}{\Phi}\right)^{1/4}$ is roughly 0.03 centimeter.

In concluding this section it should be mentioned that, although no systematic measurements of $\overline{\Delta}$ have been made, rough estimates from oscillograms in the intermittent zone of the boundary layer indicated the order of 0.05 to 0.10 times $\overline{U}_\infty$. This average velocity defect indicates the obvious fact that turbulent boundary bulges originate in a region of lower mean velocity and also represents the presence of vorticity and of locally laminar shear.

A simple mathematical model of the laminar superlayer will be taken up as a separate section in the discussion of propagation velocity of the turbulence front.

The following important inference can be made on the basis of the highly localized character of the laminar superlayer: Since no appreciable viscous effects extend beyond this thin layer, and since only viscous effects can transmit vorticity, it follows that *the mean velocity everywhere in the potential part of the flow must be constant and equal to that at "infinity."* This is a consequence of the fact that the mean vorticity is $\overline{\Omega} \doteq \partial \overline{U}/\partial y$.

This conclusion will be analytically emphasized in the following section. It is in contrast with an assumption of Townsend (ref. 10) that the nonturbulent fluid lying between bulges in the turbulence front "is constrained by pressure gradients to move at the same mean velocity" as the fluid in the adjacent turbulent bulges.

IRROTATIONALITY AND REYNOLDS SHEAR

In view of the evidence that the fluctuations outside a turbulence front are irrotational, it is pertinent to take a look at the customary turbulent-flow equations (actually valid for any stationary fluctuations) for the particular case of irrotational fluctuations. The hope is that some drastic simplification will appear.

In Cartesian tensor notation, the Reynolds equation for steady mean motion is

$$ \overline{U}_k \frac{\partial \overline{U}_i}{\partial x_k} = -\frac{1}{\rho} \frac{\partial \overline{P}}{\partial x_i} + \nu \nabla^2 U_i - \frac{\partial}{\partial x_j} \overline{(u_i u_j)} \tag{23} $$

The last term is the turbulent apparent force vector or Reynolds vector.

For irrotational fluctuations,

$$ \frac{\partial u_i}{\partial x_j} = \frac{\partial u_j}{\partial x_i} \tag{24} $$

therefore,

$$ \frac{\partial}{\partial x_j} \overline{(u_i u_j)} = \frac{1}{2} \frac{\partial \overline{(u_j u_j)}}{\partial x_i} \equiv \frac{1}{2} \frac{\partial \overline{q^2}}{\partial x_i} $$

which shows that the Reynolds force reduces to a normal force only, since it is expressible as the gradient of a scalar.

The Reynolds equation can then be written

$$ \overline{U}_k \frac{\partial \overline{U}_i}{\partial x_k} = -\frac{1}{\rho} \frac{\partial}{\partial x_i} \left(\overline{P} + \frac{\rho}{2} \overline{q^2} \right) + \nu \nabla^2 \overline{U}_i \tag{25} $$

and this form emphasizes the fact that, regardless of the mean velocity field, *irrotational fluctuations give no net apparent shear forces on a fluid element.*[3]

This does not necessarily mean, however, that the Reynolds shear force on a plane is zero or that the Reynolds stress tensor $-\rho \overline{u_i u_k}$ has only leading diagonal terms. Also there may still be a continuous "production" of fluctuating kinetic energy, that is, a transfer from the mean motion kinetic energy $\left(\overline{u_i u_k} \frac{\partial \overline{U}_i}{\partial x_k} \neq 0 \right)$.

[3] This fact was pointed out by Dr. F. H. Clauser.

Comparison of equations (23) and (25) for the case of motion two-dimensional in the mean (three-dimensional irrotational fluctuations) yields the relations for the Reynolds shear force components

$$\frac{\partial \overline{uv}}{\partial y}=\frac{1}{2}\frac{\partial}{\partial x}(\overline{v^2}+\overline{w^2}-\overline{u^2}) \tag{26}$$

$$\frac{\partial \overline{uv}}{\partial x}=\frac{1}{2}\frac{\partial}{\partial y}(\overline{u^2}+\overline{w^2}-\overline{v^2}) \tag{27}$$

which may also be regarded as a pair of differential equations relating the four nonzero components of the Reynolds stress tensor.

Two provocative forms follow from alternative combinations of equations (26) and (27):

$$\frac{\partial^2 \overline{uv}}{\partial x^2}-\frac{\partial^2 \overline{uv}}{\partial y^2}=\frac{\partial^2}{\partial x\,\partial y}(\overline{u^2}-\overline{v^2}) \tag{28}$$

and

$$\frac{\partial^2 \overline{uv}}{\partial x^2}+\frac{\partial^2 \overline{uv}}{\partial y^2}=\frac{\partial^2 \overline{w^2}}{\partial x\,\partial y} \tag{29}$$

Equation (28) gives the interesting conclusion that if $\overline{u^2}-\overline{v^2}$ is constant in either x or y the turbulent shear stress satisfies a homogeneous plane-wave equation with characteristics at $\pm 45°$ in the xy-plane.

For the particular flows studied in this report, the experimental results show that $\overline{uv}$ approaches zero faster than $u'v'$ as y (or r) is increased. This seems to indicate that $\overline{uv}=0$ in the potential field. However, insufficient coverage and accuracy of the data preclude the possibility of checking this through equation (28). Since $\overline{uv}=\overline{u^2}=\overline{v^2}=0$ for $y=\infty$, such a check would require that $\overline{u^2}=\overline{v^2}$ throughout the potential field.

Parenthetically, viscous fluids with zero net shear force on a fluid element but with nonzero shear stress are far from unknown mathematically: Any irrotational laminar flow of a viscous fluid is such a case (aside from the trivial case of $\overline{Q}=$Constant). The requirement on a stress tensor σ_{ik} that it produce only normal forces is that

$$\frac{\partial \sigma_{ik}}{\partial x_k}=\frac{\partial G}{\partial x_i} \tag{30}$$

where G is a scalar.

The principal significance of equation (25) in the general problem under investigation is as follows: Assuming that the fluctuations on the free-stream side of the turbulence front are actually irrotational, as both measurements and heuristic reasoning indicate, the mean velocity there must be equal to that for $y=\infty$. This verifies the physical inference drawn in the previous section from the concept of the localized laminar superlayer.

It appears paradoxical that the mean flow kinetic energy should be unchanged in a zone where there has appeared an appreciable kinetic energy in velocity fluctuations. However, the latter can come from the turbulent part of the field through nonviscous effects, leaving mean flow kinetic energy in the potential zone unchanged. This would be consistent with the inference that $\overline{uv}=0$.

Probably the highest intensity random irrotational fluctuations easily available in the laboratory are those in the "potential cone" of a round turbulent jet. These apparently get as high as $u'/\overline{U}\approx 5$ percent (ref. 2).

Equation (28) also can be deduced for the special case of a constant mean velocity field with arbitrary fluctuations, provided only that the mean values are plane, that is, $\frac{\partial}{\partial z}\overline{(\ )}=0$.

THEORETICAL BEHAVIOR OF TURBULENCE FRONT

As mentioned in the "Introduction," two of the fluid mechanically pertinent characteristics of the relatively sharp boundary between turbulent and nonturbulent fluid are (a) its mean rate of increase of wrinkle amplitude in the downstream direction and (b) its mean velocity of propagation transversely into the irrotational fluid. The following sections represent crude theoretical attempts to predict these two characteristics in terms of the statistical properties of the fully turbulent fluid on one side of the boundary.

WRINKLING RATE

In turbulent flows with R_λ greater than about 10, there is no reason to expect any particular chunk of fluid to return to the nonturbulent state once it has become turbulent. Therefore, the presence of turbulence in a small piece of fluid can be regarded as an indelible tagging, somewhat like heat or a chemical contaminant. Were it not for the continuous propagation of the turbulence front into new fluid, this front would always consist of the same fluid particles and would obviously be susceptible to a Lagrangian study in terms of Taylor's theory of diffusion by continuous movements (ref. 20), as has been applied to the wrinkling rate (identical to turbulent diffusion rate) of a very thin sheet of thermally tagged fluid in a turbulent flow (refs. 1 and 18).

In fact, a uniform translational velocity $\overline{V^*}$ of the tagging attribute relative to the fluid does not render Taylor's concepts invalid; it does, however, require a generalization of the analysis to a mixed Eulerian and Lagrangian treatment, though somewhat different from the relative dispersion case set up by Brier (ref. 21) and by Batchelor (ref. 22). Clearly in the limit of $\overline{V^*}\gg v'$ (e. g., wrinkling of a Mach wave propagating through low-speed turbulence) it reduces to a simple Eulerian diffusion problem, while in the limit of $\overline{V^*}\ll v'$ the purely Lagrangian analysis of Taylor applies.

For the present problem it appears that neither of these limiting conditions holds, although the latter is closer. Consider the rough-wall boundary layer at $x=102$ inches as an example:

$$\frac{\overline{V^*}}{v'}\approx\frac{\overline{U}}{v'}\times\frac{d}{dx}(\overline{Y}-\delta^*)\approx 0.1$$

where $v'/\overline{U}$ is taken in the fully turbulent zone adjacent to the intermittent zone. This formula is deduced in the section "Applications to Particular Turbulent Flows."

Since the basic problem (diffusion of a front propagating through a homogeneous turbulence) has yet to be analyzed, the present phenomenon will be estimated as though

$\overline{V^*} \ll v'$. Subsequent approximations are consistently rough.

Another peculiar property of the present problem is that the surface whose turbulent diffusion is of interest has turbulent flow on only one side; the thermally tagged surface used in conventional diffusion studies has the same kind of turbulence on both sides. However, the theory of diffusion by continuous movements is simply a kinematic analysis based on the presumably given velocity statistics of the fluid particles in the surface. If these are correctly given, no further information or restriction is necessary. Therefore, since the purpose of this section is to predict the form of $\sigma(x)=\sqrt{\overline{(Y-\overline{Y})^2}}$ in terms of the properties of the fully turbulent zone, the only additional assumption necessary is that the velocity fluctuations of the fluid particles in the front are proportional to those in the fully turbulent fluid near the front.

The analysis of one-dimensional diffusion by continuous movements for a homogeneous field with no mean motion leads to

$$\frac{d\sigma^2}{dt}=2(v')^2\int_0^t R_L(\tau)\,d\tau \tag{31}$$

where σ is the standard deviation of the distance traveled due to turbulent convection and R_L is the Lagrangian correlation coefficient. For times long compared with that for which $R_L \approx 0$, the familiar asymptotic form results:

$$\sigma(t)=v'\sqrt{2L_t t} \tag{32}$$

where $L_t \equiv \int_0^\infty R_L dt$ is the Lagrangian (time) scale.

If a relatively high uniform mean velocity in the x-direction is introduced ($\overline{U} \gg v'$), equations (31) and (32) can be interpreted approximately in spatial terms since $\overline{U}t \approx x$ for any particle (refs. 1, 18, and 23). Then

$$\sigma(x) \approx \frac{v'}{\overline{U}}\sqrt{2\Lambda_L x} \tag{33}$$

where $\Lambda_L \equiv \overline{U}L_t$ is an approximate longitudinal Lagrangian length scale.

It has been pointed out in previous publications (refs. 18 and 24) that the most concise representation in such a flow follows from introduction of a transversal Lagrangian length scale $L_L \equiv v'L_t$. Then

$$\sigma(x) \approx \sqrt{2\left(\frac{v'}{\overline{U}}\right)L_L x} \tag{34}$$

which gives the dispersion (identical to surface wrinkle amplitude) at large distances from a fixed source of tagging, when $v(t)$ following a fluid particle is a stationary random variable and $\overline{U}$ is constant.

For the hypothetical case of the turbulence front bounding a turbulent motion homogeneous in the stream direction, this asymptotic form would pertain; the "source" lies indefinitely far upstream. However, in virtually all turbulent flows of interest, the statistical properties of the motion vary with x. Consequently, application of equation (34) to these cases implies the further restriction that these x-variations be slow, that is, that there be little change in an x-interval comparable with Λ_L

A particular example of the degree of validity of this restriction can be drawn from the case of decaying isotropic turbulence, where Lagrangian scales have actually been measured (ref. 18). At 43 mesh lengths behind a 1-inch-square mesh grid of ¼-inch dowel, with $\overline{U}=25.8$ feet per second, it is found that $v'/\overline{U}=2.0$ percent, $\Lambda_L \approx 17$ inches, and dv'/dx corresponds to a change of about ⅛ in $v'/\overline{U}$ over an x-interval equal to Λ_L. However, $\frac{1}{L_L}\frac{dL_L}{dx}\Lambda_L$ is only on the order of 0.03.

In most shear flows, the $v'/\overline{U}$ changes will be slower than for this decaying isotropic turbulence while the L_L changes may be slightly faster. In general, it can be anticipated that in the application of equation (34) to boundary layer, jet, and wake the requirement of slow x-variations in turbulence properties will be satisfied at least as well as the previously mentioned restrictions for this Lagrangian treatment. These applications and comparison of computed values of $\sigma(x)$ with experimental results will be presented further along, under the appropriate section headings.

PROPAGATION VELOCITY BY DIMENSIONAL REASONING

The average velocity of propagation of the laminar superlayer (or turbulence front) relative to the local fluid $\overline{V^*}$ must be monotonic with the average magnitude of the instantaneous (laminar) shear stress in the superlayer $\left(\text{proportional to } \mu\frac{\Delta}{\epsilon}\right)$. However, the ratio is not a directly measurable quantity and must be replaced by something more tractable. As has been mentioned in the section "Laminar Superlayer," when there is no mean shear stress Δ/ϵ must be of the same order as the vorticity fluctuations in the turbulent fluid near the front. Therefore $\overline{V^*}$ should be monotonic in ω'. Since this is a viscous phenomenon, it must also depend upon ν.

In fact, the inference that $\overline{V^*}=\overline{V^*}(\nu, \omega')$ can be made on a much more direct and superficial level. Since the laminar superlayer is a device for the viscous propagation of vorticity fluctuations into an irrotational fluid (in the case of zero mean shear), the propagation velocity must depend at least on ω' and on ν. Furthermore, these alone are sufficient to produce a parameter with the dimensions of velocity.

The only combination giving the appropriate dimensions gives, by inspection,

$$\overline{V^*} \propto \sqrt{\nu\omega'} \tag{35}$$

for zero mean shear stress.[4] Of course, $\overline{V^*}$ is directed perpendicular to the local tangent plane of the turbulence front. The effects of nonplanarity of the whole front will be noted later in this section.

Equation (35) would be expected to apply, for example, in the case of the boundary between a homogeneous turbulence and a nonturbulent fluid, with $\overline{U}$ constant over the entire flow field.

At the free boundary of a turbulent shear flow it is to be expected that the shear force vector of the laminar superlayer will have a mean value which will also promote $\overline{V^*}$.

[4] It should also be noted that the assumption that R_ϵ (where $R_\epsilon \equiv \bar{\epsilon}^2\omega'/\nu$) has a "universal" average value corresponding to a lower critical Reynolds number coincides with the plausible dimensional hypothesis that $\bar{\epsilon} \propto \sqrt{\nu/\omega'}$.

If the whole front were nearly flat, this mean value would be a function of y in the superlayer and also proportional to the mean shear in the turbulent fluid just inside the turbulence front,[5] varying from equality on the turbulent edge to zero on the free-stream side. Sketch (b) includes this concept in a coordinate system attached to the laminar superlayer.

In this more general case, the physical picture suggests that $\overline{V^*}$ depends upon the average magnitude of the total shear in the superlayer: $\overline{V^*}=\overline{V^*}(\overline{S^2})$, where $\underline{S}(t)=\overline{\underline{S}}+\underline{s}(t)$ is the shear force vector on a unit area on the turbulent edge of the superlayer. With Cartesian coordinate system x_1, y_1, and z_1 fixed in and alined with the turbulence front (y_1 perpendicular to front), the fluctuation $\underline{s}$ has only x_1- and z_1-components. Then, with gross mean shear directed along x_1, $\overline{S^2}=\overline{S_{x_1}}^2+\overline{s_{x_1}^2}+\overline{s_{z_1}^2}$.

Dimensional reasoning gives

$$\overline{V^*}\propto\sqrt{\frac{\overline{S'}}{\rho}}=\left(\frac{\overline{S_{x_1}}^2+\overline{s_{x_1}^2}+\overline{s_{z_1}^2}}{\rho^2}\right)^{1/4} \tag{36}$$

If the random slope of the turbulence front in the x-, y-, and z-coordinates is small on the average, the x_1-, y_1-, and z_1-system can be replaced by x, y, and z, and $\overline{S_{x_1}}$ is proportional to the mean shear stress in the turbulence. Furthermore, with local isotropy in the turbulence, $\overline{s_{x_1}^2}\approx\overline{s_{z_1}^2}$. As in the simpler case, these are proportional to $(\omega')^2$. Then equation (36) can be written

$$\overline{V^*}\propto\left[\frac{\overline{S_x}^2+B\mu^2(\omega')^2}{\rho^2}\right]^{1/4} \tag{37}$$

where B is a numerical constant, probably of order unity. This reduces to equation (35) for a shear-free turbulence. For each particular type of turbulent shear flow, $\overline{S_x}$ can be taken proportional to some characteristic mean shear stress. No application of equation (36) or (37) is made later in this report.

Handling of the propagation problem in terms of a plane turbulence front implies that $\bar{\epsilon}$ is much smaller than the radii of curvature of the front. The degree of validity of this assumption is not easy to check directly from the statistics of the turbulent fluid; it requires fairly detailed information on $Y(x,t)$. However, the measurements on statistical distribution of pulse lengths coming out of the trigger circuit (fig. 29), transformed by $\overline{U}_\infty$ from time to length, give indirect indication that the assumption is well satisfied.

Conversely, since $\overline{V^*}$ is normal propagation velocity of the front (especially in the case with zero mean shear), propagation with constant $\overline{V^*}$ over the whole front would tend to introduce a skewness into the probability density of Y, as in sketch (c). This is the effect mentioned by Karlovitz (ref. 26) in accounting for the skew nature of the flame front as observed in a turbulent bunsen flame.

The highly symmetrical shape of $\partial\gamma/\partial y$ (indicated by linearity in fig. 32) shows that this effect, if present, is negligible in the phenomenon considered here.

[5] In fact, F. H. Clauser proposes a propagation velocity, for the turbulent boundary layer, depending only on the mean shear stress in the turbulence: $\overline{V^*}\propto\tau_w/\rho\overline{\Delta}$ (ref 25).

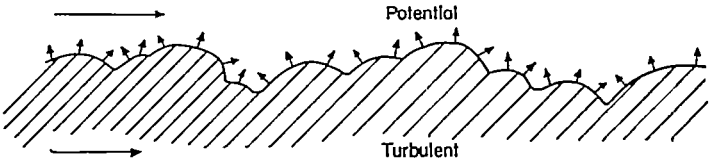

Sketch (c).

This negligibility is an indication that the radii of curvature of the front are large compared with the wave lengths. This means that $\overline{V^*}$ is directed very nearly perpendicular to the $\overline{Y}(x)$ surface. For two-dimensional flows in which the boundary-layer approximation applies, this in turn is nearly parallel to the xz-plane, that is, $d\overline{Y}/dx\ll 1$. Therefore, within a corresponding approximation, the surface area of the turbulence front on a two-dimensional flow is equal to its projection on the xz-plane, and the average rate of conquest of new fluid by the turbulent state is $\overline{V^*}$, in units of volume per unit time per unit area of contact. A similar concept holds for the axially symmetric flows.

It is obvious that a turbulent shear flow can have similarity only if both $\sigma(x)$ and $\overline{Y}(x)$ are proportional to the boundary-layer thickness $\delta(x)$ (which, of course, must be proportional to any other characteristic thickness defined in terms of the mean velocity profile). Stated in different but related terms, the average rate of flow of turbulent fluid passing through any constant x-plane must be proportional to the rate of flow of boundary-layer fluid passing through the plane.

MODEL OF LAMINAR SUPERLAYER

Dimensional reasoning as employed in the preceding section, and in earlier ones, gives at best the functional forms of the laminar-superlayer characteristics in terms of the statistical properties of the turbulence with which it is associated. Fully quantitative results follow only through deductive analysis, that is, actual solution of an appropriate boundary-value problem. Since the actual problem appears to be too complex for full solution at present, a simple physicomathematical model will be used with the expectation that the results, after interpretation in terms of pertinent variables in the actual problem, will give a proper order-of-magnitude relation among these variables.

The model proposed is a generalization of the Stokes and Rayleigh problem of the infinite wall moving in its own plane (ref. 27). The first extension is the addition of a constant suction velocity $\overline{V}(<0)$ with, of course, wall porosity. The velocity $\overline{V}$ corresponds to propagation velocity of the turbulence front. The differential equations are thus

$$\frac{\partial U}{\partial t}+\overline{V}\frac{\partial U}{\partial y}=\nu\frac{\partial^2 U}{\partial y^2} \tag{38a}$$

$$\frac{\partial W}{\partial t}+\overline{V}\frac{\partial W}{\partial y}=\nu\frac{\partial^2 W}{\partial y^2} \tag{38b}$$

Since the U and W equations are independent they can be treated separately. In the absence of mean shear they are identical, and only one need be considered.

Since equations (38) are linear, the vorticity components $Z \equiv \partial U/\partial y$ and $\Xi \equiv \partial W/\partial y$ obey the same equations as the velocities:

$$\frac{\partial Z}{\partial t}+\overline{V}\frac{\partial Z}{\partial y}=\nu\frac{\partial^2 Z}{\partial y^2} \tag{39a}$$

$$\frac{\partial \Xi}{\partial t}+\overline{V}\frac{\partial \Xi}{\partial y}=\nu\frac{\partial^2 \Xi}{\partial y^2} \tag{39b}$$

These equations are to be solved with boundary conditions

$$Z(t,\infty)=\Xi(t,\infty)=0 \tag{40a}$$

$$Z(t,0)=\overline{Z}_o+\zeta_o \sin \alpha t \tag{40b}$$

$$\Xi(t,0)=\xi_o \sin \beta t \tag{40c}$$

Since Ξ has only a fluctuating part, and since linearity permits separation of the steady and fluctuating parts of Z, the problem becomes

$$\overline{V}=\frac{d\overline{Z}}{dy}=\nu\frac{d^2\overline{Z}}{dy^2} \tag{41}$$

with $\overline{Z}(\infty)=0$ and $\overline{Z}(0)=\overline{Z}_o$, and

$$\frac{\partial \zeta}{\partial t}+\overline{V}\frac{\partial \zeta}{\partial y}=\nu\frac{\partial^2 \zeta}{\partial y^2} \tag{42}$$

with $\zeta(t,\infty)=0$ and $\zeta(t,0)=\zeta_o \sin \alpha t$. There is an identical boundary-value problem for $\xi(t,y)$.

To get closer equivalence to the fully three dimensional problem a purely mathematical extension can be made, corresponding roughly to the physical phenomenon of continuous vorticity fluctuation production (by fluid-line stretching) at a rate proportional to that already present. This is most simply done by adding a linear term to the ξ equation, giving

$$\frac{\partial \zeta}{\partial t}+\overline{V}\frac{\partial \zeta}{\partial y}=\nu\frac{\partial^2 \zeta}{\partial y^2}+K\zeta \tag{43}$$

where K is like a constant average vortex-line stretching rate.

No corresponding term is added to equation (41) because the plane form of the mean-vorticity equation for turbulent flow (eq. (9)) shows no term identifiable as production of mean vorticity due to random turbulent stretching of vortex lines.

The solution of equation (41) is

$$\overline{Z}=\overline{Z}_o \exp\left(\frac{\overline{V}}{\nu}y\right) \qquad (\overline{V}<0) \tag{44}$$

The solution of equation (43) is

$$\zeta=\zeta_o \exp\left[\left(\frac{\overline{V}}{2\nu}-\frac{1}{\sqrt{2}}\left\{\sqrt{\left[\left(\frac{\overline{V}}{2\nu}\right)^2-\frac{K}{\nu}\right]^2+\left(\frac{\alpha}{\nu}\right)^2}+\left(\frac{\overline{V}}{2\nu}\right)^2-\frac{K}{\nu}\right\}^{1/2}\right)y\right]\times\sin\left[\alpha t-\frac{1}{\sqrt{2}}\left\{\sqrt{\left[\left(\frac{\overline{V}}{2\nu}\right)^2-\frac{K}{\nu}\right]^2+\left(\frac{\alpha}{\nu}\right)^2}-\left(\frac{\overline{V}}{2\nu}\right)^2+\frac{K}{\nu}\right\}^{1/2}y\right] \quad (\overline{V}<0;\ \alpha, K>0) \tag{45}$$

with a similar expression for ξ. Here the negative root has been chosen so that equation (45) reduces to Stokes' solution for $\overline{V}=K=0$.

From equations (44) and (45) it is desirable to extract an expression for the thickness of the disturbed layer. A convenient measure of thickness is simply the inverse of the coefficient of $-y$ in the exponentials of both solutions:

$$\epsilon_1=-\frac{\nu}{\overline{V}} \tag{46}$$

$$\epsilon_2=\frac{1}{-\frac{\overline{V}}{2\nu}+\frac{1}{\sqrt{2}}\left\{\sqrt{\left[\left(\frac{\overline{V}}{2\nu}\right)^2-\frac{K}{\nu}\right]^2+\left(\frac{\alpha}{\nu}\right)^2}+\left(\frac{\overline{V}}{2\nu}\right)^2-\frac{K}{\nu}\right\}^{1/2}} \tag{47}$$

Application of equations (46) and (47) to the laminar-superlayer problem requires identification of $\overline{V}$, α, and K with measurable variables in the turbulent fluid near the superlayer:

(1) $-\overline{V}\approx\overline{V^*}$, the propagation velocity.

(2) $\alpha\approx\xi'$, the root-mean-square value of any one of the three orthogonal turbulent vorticity fluctuation components. In other words, root-mean-square vorticity may be regarded as a characteristic frequency of turbulence. For large values of R_λ, $\xi'\approx\eta'\approx\zeta'$ by local isotropy.

(3) $K\approx\sqrt{\overline{\left(\frac{\partial u}{\partial x}\right)^2}}\approx\sqrt{\overline{\left(\frac{\partial v}{\partial y}\right)^2}}\approx\sqrt{\overline{\left(\frac{\partial w}{\partial z}\right)^2}}$ for large R_λ's. Hence, with local isotropy, $K\approx\xi'/\sqrt{5}$ is a measure of the rate of fluid-line stretching.

Substituted into equations (46) and (47), these give

$$\epsilon_1\approx\frac{\nu}{\overline{V^*}} \tag{48}$$

$$\epsilon_2\approx\frac{1}{\frac{\overline{V^*}}{2\nu}+\frac{1}{\sqrt{2}}\left\{\sqrt{\left[\left(\frac{\overline{V^*}}{2\nu}\right)^2-\frac{\xi'}{\nu\sqrt{5}}\right]^2+\left(\frac{\xi'}{\nu}\right)^2}+\left(\frac{\overline{V^*}}{2\nu}\right)^2-\frac{\xi'}{\nu\sqrt{5}}\right\}^{1/2}} \tag{49}$$

A simpler, more approximate form for ϵ_2 is attained after inspection of the experimental orders of magnitude of $\overline{V^*}$ and ξ'. For example, at the inner side of the intermittent zone, in the rough-wall boundary layer at $x=102$ inches, $\overline{V^*}\approx 1.3$ inches per second and $\xi'\approx 400$ per second. Therefore, it turns out that equation (49) can be simplified by liberal employment of chopped-off binominal expansions. The roughest (and simplest) resulting estimate is

$$\epsilon_2\approx\sqrt{\frac{\nu}{\xi'}} \tag{50}$$

Since the laminar superlayer can be assumed to exist even in the absence of a mean vorticity field, it is reasonable to assume that the fluctuating part of the superlayer model is the more pertinent one. Then one may take ϵ_2 to be $\bar{\epsilon}$, giving the theoretical prediction

$$\bar{\epsilon}\approx\sqrt{\frac{\nu}{\xi'}} \tag{50a}$$

as an order of magnitude. This is consistent with the earlier conjecture on the constancy and order of a possible Reynolds

number $R_\epsilon \equiv \bar{\epsilon}^2\omega/\nu$. It does not appear to be susceptible to direct experimental verification, but, as mentioned earlier, is of the same order as the Kolmogoroff (minimum) length

$$\bar{\epsilon} \approx \chi \equiv \left(\frac{\nu^3}{\bar{\Phi}}\right)^{1/4} \tag{51}$$

which follows from equation (50a) and the relation between χ and λ.

No estimate of $\overline{V^*}$ follows from equation (50) and, insofar as a strictly fluctuating laminar superlayer is concerned, the dimensionally induced equation (35) remains as sole prediction of propagation velocity.

However, equation (48) for the mean thickness gives

$$\overline{V^*} \approx \frac{\nu}{\epsilon_1} \tag{52}$$

If there is a single layer, $\overline{V^*}$ should be the same for both fluctuating and average vorticity. If ϵ_1 happened to be of the same order as ϵ_2, equations (51) and (52) would give $\overline{V^*} \approx 0(\sqrt{\nu\xi'})$, but there seems to be insufficient a priori basis to make this guess a formal part of the analysis.

INFERENCE OF TURBULENCE PROPERTIES FROM INTERMITTENT SIGNAL

Townsend (refs. 10 and 28) has suggested that it may be possible to compute the statistical properties of the turbulence inside the convex bulges of the turbulence front from a knowledge of the corresponding statistical properties of the full intermittent signal plus the intermittency factor γ. His hypothesis is that, in effect,

$$\overline{a_T^2} = \frac{\overline{a^2}}{\gamma} \tag{53}$$

where $a(t)$ is a random property of the flow and a_T is the same property but confined to the turbulent parts of the total signal. For example, Townsend refers to $\dfrac{\overline{u^2}+\overline{v^2}+\overline{w^2}}{\gamma}$ as "the mean turbulent intensity within the jets" (identical to bulges).

Actually, the applicability of equation (53) is contingent upon very definite restrictions. For discussion purposes, suppose that $a(t)$ is the complete signal and $b(t)$ is the intermittent (0 or 1) signal. Obviously, $\overline{b}=\overline{b^2}=\gamma$, the intermittency factor. Also $a_T(t)$ is a hypothetical signal whose physical nature is the same as $a(t)$ but applies to turbulent fluid only. If a_T is chosen to have a mean value of zero, then it is necessary to introduce a constant quantity A which is the distance between the zero line of $a_T(t)$ and the signal level corresponding to $b(t)$ at zero.

Sketch (d) illustrates the definitions. Implicit in this formulation and sketch is the restriction that a (or a_T) is a physical property which is zero in the potential flow region.

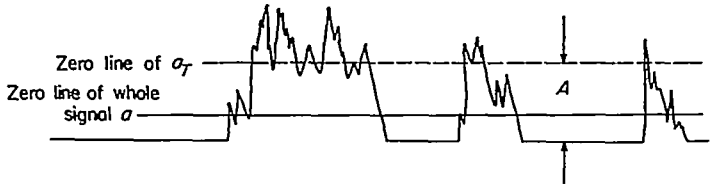

Sketch (d).

With this representation, the total signal expressed in terms of the other quantities is

$$a(t) = b(t)[a_T(t)+A] - \overline{ba_T} - A\gamma \tag{54}$$

since $\bar{a}=0$ by definition and $\overline{b(a_T+A)}=\overline{ba_T}+A\gamma$. Whence, the mean-square value can be written as

$$\overline{a^2} = \overline{b^2a_T^2} + 2A\overline{b^2a_T} - \overline{(ba_T)}^2 - 2A\gamma\overline{ba_T} + \gamma(1-\gamma)A^2 \tag{55}$$

The objective is to express $\overline{a_T^2}$ as a function of $\overline{a^2}$ and other necessary parameters. Obviously this is impossible without introducing some further restrictions, especially on the statistical relation between $a_T(t)$ and $b(t)$. Therefore, assume

$$\left.\begin{aligned} &\text{(a) } \overline{ba_T}=0 \text{ (whence } \overline{b^2a_T}=0, \text{ since } b^2=b \\ &\text{(b) } \overline{b^2a_T^2}=\overline{b^2}\times\overline{a_T^2}=\gamma\overline{a_T^2} \end{aligned}\right\} \tag{56}$$

A sufficient but not necessary condition for these two is that $b(t)$ and $a_T(t)$ be statistically independent.

With restrictions (56), equation (55) reduces to

$$\overline{a^2} = \gamma\overline{a_T^2} + \gamma(1-\gamma)A^2 \tag{57}$$

and the turbulence property $\overline{a_T^2}$ can be computed from the corresponding total-signal property plus measurements of γ and A.

For some physical variables $a(t)$ it will turn out that $A=0$ and then equation (57) reduces to equation (53).

For the quantity $\overline{a_T^2}$ to have any simple interpretation it must of course be assumed that the physical variable it represents is a homogeneous random variable in the turbulent fluid.

Summarizing the conditions necessary for equation (53) to lead to meaningful results, the following restrictions are necessary:

(1) The physical variable must be zero in the potential flow.

(2) The physical variable must be homogeneous in the turbulent flow.

(3) The physical variable (and its square) in the turbulent flow must be uncorrelated with the location of the front.

(4) There must be no mean value in the variable between turbulent and potential flows for the same value of y.

The first condition immediately eliminates velocity fluctuations from this sort of treatment. This renders uncertain Townsend's turbulent energy application, mentioned above. However, vorticity fluctuation and turbulent shear certainly satisfy it, as may temperature or concentration fluctuations and heat or mass transfer, when these are present.

The second requirement is probably not satisfied by any variables in flows with transport, including, of course, the commonest example, shear flow. This follows from the fact that, even in spatial zones with $\gamma=1$ everywhere, there are gradients in all of the quantities which have been measured. Consequently, the entire concept of $\overline{a_T^2}$ as a function of position in a shear flow must be semiquantitative at best.

It seems unlikely that the third requirement is satisfied by all of the physical variables, but for most of them it may be close enough that equation (57) would be approximately true.

Finally, the occurrence of a mean value between potential and turbulent fluid must also depend upon the particular physical variable under consideration. It certainly does occur for longitudinal velocity at the boundary of a turbulent shear flow. It certainly does not occur for z-component velocity in a shear flow which is two-dimensional in the mean with gradients all in the x- and y-directions. For many physical variables its occurrence or absence is not a priori obvious. In any case it can be handled by resorting to equation (57).

For complex cases, when even equation (57) is believed to be inadequate, possibly because the variable is not zero in the potential zone, it is still possible to obtain statistical information on the signal structure within the turbulent bursts by laborious computational procedure for the oscillographic trace.

A more detailed question may be raised at this point as to the influence of intermittency upon the measured power spectrum of velocity fluctuation. Again the answer is certain to be simple if the four conditions listed above are satisfied. In that case, with probe signal $a(t)=a_T(t)b(t)$, the autocorrelation functions of the three variables are related by

$$\psi_a(\tau)=\psi_{a_T}(\tau)\psi_b(\tau) \tag{58}$$

where τ is time interval. The power spectra are simply the Fourier cosine transforms of the correlations and, since the transform of a product is equal to the convolution integral of the individual transforms, the three power spectra are related by

$$F_a(n)=\int_0^\infty F_{a_T}(n_1)F_b(n-n_1)dn_1 \tag{59}$$

where $F_a(n)$ can be measured directly from the output of the hot-wire anemometer; $F_b(n)=F_c(n)$, the spectrum of the Schmitt trigger output in the intermittency-measuring circuit (see fig. 28); and $F_{a_T}(n)$ is the spectrum of a hypothetical homogeneous turbulence variable which should give the nature of the fluctuations within the bulges of the wrinkled front.

Equation (59) is a Fredholm integral equation of the first kind, readily solved in principle by Fourier integral methods—which corresponds in effect to going back to equation (58).

No attempt has been made to apply this relation because the experimental results appear too uncertain to merit such detailed manipulation. It is hoped, however, that such a study can be made in later shear-flow research.

APPLICATIONS TO PARTICULAR TURBULENT FLOWS

Application of the foregoing general concepts and theoretical predictions on the behavior of the turbulence front to particular turbulent flows involves two explicit aspects:

(a) Comparison of directly measured $\sigma(x)$ and $\overline{Y}(x)$ with measured values of characteristic shear-layer thicknesses, for example, $\theta(x)(\propto\delta^*\propto\delta)$ in the boundary layer.

(b) Comparison of $\sigma(x)$ and $\overline{Y}(x)$, as computed from measured turbulence data, with directly measured values of $\sigma(x)$ and $\overline{Y}(x)$.

The first step is the strictly experimental process of examining a new aspect of the degree of similarity to be found in the detailed structures of the various turbulent shear flows.

The second has as its purpose the approximate verification of the rather crude hypotheses leading to prediction of the turbulence front behavior, that is, to equations such as (34) and (35).

ROUGH-WALL BOUNDARY LAYER

Fitting the experimental results on boundary-layer thickness by a simple power-law relation (see appendix), it turns out that, neglecting Reynolds number effects,

$$\delta\propto\delta^*\propto\theta\propto(x-x_o)^{0.61\pm0.1} \tag{60}$$

numerically,

$$\left.\begin{aligned}\delta&\approx0.19(x-x_o)^{0.61}\text{ in.}\\ \delta^*&\approx0.13(x-x_o)^{0.61}\text{ in.}\\ \theta&\approx0.026(x-x_o)^{0.61}\text{ in.}\end{aligned}\right\} \tag{60a}$$

The fitting of a power law to a set of points without origin involves two steps: (1) An origin must be chosen by trial and error to give the closest approximation to linearity on logarithmic graph paper, and (2) the "best" straight line must be drawn through the resulting plot. This procedure was also applied to the fitting of power-law approximations to the experimental data on $\sigma(x)$ and $\overline{Y}(x)$. Figure 21 illustrates the degree to which a power-law fitting is successful. The latter quantities are then given by this "direct" measurement as

$$\sigma\approx0.022(x-x_o)^{0.67\pm0.1}\text{ in.} \tag{61}$$

$$\overline{Y}\approx0.14(x-x_o)^{0.63\pm0.1}\text{ in.} \tag{62}$$

The "best" common origin is $x_o=-20$ inches.

Comparison of equations (61) and (62) with equation (60) shows that, within the precision of these experimental results, the turbulence front both progresses laterally and increases in amplitude at the same rate as the mean boundary-layer flow grows. The uncertainty range indicated is a crude estimate of standard deviation, not the maximum.

Verification of equation (34) requires knowledge of both $v'/\overline{U}$ and L_L (the transversal Lagrangian scale) as functions of x. On the basis of the $v'/\overline{U}$ measurements at corresponding positions across the boundary layer at four different x-stations (fig. 17), it is assumed for the sake of this calculation that $v'\propto U_\tau$, as dimensional reasoning and Laufer's pipe measurements (ref. 15) also indicate. The U_τ is obtained from the measurements of $\theta(x)$: $U_\tau\propto x^{-0.20}$ for very large values of x.

Unfortunately, there exist no measurements of Lagrangian scale in turbulent shear flows. However, the ratio of Lagrangian to Eulerian scale L_L/L has been measured as a function of $v'L/\nu$ for isotropic turbulence (ref. 18). These highly scattered measurements show L_L/L to be a slowly decreasing function of $v'L/\nu$. In order to estimate $L_L(x)$ for substitution into equation (34) it is assumed that this variation holds roughly for shear flow. Further, there is

good evidence that for a given shear flow the Eulerian scale is proportional to the characteristic width of the shear zone; that is, in this case, $L \propto \delta$ and the constant of proportionality is taken from the smooth-wall boundary layer of Schubauer and Klebanoff (ref. 4) at a station where $d\overline{P}/dx = 0$. Their data give $L \approx 0.17\delta$.

With this estimate of L/δ, $v'L/\nu$ in the present boundary layer goes from about 300 to 500 in the principal test area: 20 inches$<x<$110 inches. But over this range of $v'L/\nu$, figure 34 of reference 18 indicates (by extrapolation) little change in L_L/L. Therefore, for purposes of the present rough estimate, it is assumed that $L_L \propto L \propto \delta$. With $\delta \propto x^{0.61}$ (eq. (60)) and $v' \propto U_\tau \propto x^{-0.20}$, the resulting theoretical prediction (eq. (34)) is

$$\sigma(x) \propto (x - x_o)^{0.7} \tag{63}$$

which agrees with the directly measured exponent (eq. (61)) perhaps better than the accuracy of either measurement or theoretical approximation.

Verification of equation (35) requires information only on $\xi'(x)$ at corresponding y-positions in the boundary layer. Since this information is not yet directly available, one assumes the isotropic relation $\xi' \approx \sqrt{5}\,\frac{v'}{\lambda}$, where $v'(x)$ has been measured and $\lambda(x)$ can be inferred by using the well-known isotropic estimate[6] $\frac{\lambda}{L} \approx \left(\frac{7\nu}{v'L}\right)^{1/2}$ and assuming $L \approx 0.17\delta$ as before. Using the experimental value of $\delta(x)$ (eq. (60a)), this calculation gives

$$\overline{V^*}(x) \propto (x - x_o)^{-0.30}\overline{U}_\infty \tag{64}$$

For comparison with experiment this is next translated into $\overline{Y}(x)$. Since $\overline{V^*}$ is propagation velocity relative to the fluid, one can write the approximate relation

$$\frac{d\overline{Y}}{dx} \approx \frac{V(\overline{Y}) + \overline{V^*}}{\overline{U}(\overline{Y})} \tag{65}$$

which should hold for any reasonably flat turbulence front. The term $\overline{V}$ is the mean fluid velocity in the y-direction. Equation (65) is approximate because (a) in some flows the front is not very flat and (b) at $y = \overline{Y}$ the mean velocity of the turbulent fluid is somewhat less than that of the nonturbulent fluid (i. e., $\overline{U}_\infty$).

For the boundary layer, it is well known that

$$\frac{d\delta^*}{dx} \approx \frac{\overline{V}(\delta)}{\overline{U}_\infty} \tag{66}$$

which is easily shown from the definition of $\delta^*(x)$.

Since experiments show that $\overline{U}(\overline{Y}) \approx \overline{U}(\delta) = \overline{U}_\infty$, one can infer $\overline{V}(\overline{Y}) = \overline{V}(\delta)$, so that, for the boundary layer, equation (65) gives

$$\frac{d\overline{Y}}{dx} \approx \frac{\overline{V^*}}{\overline{U}_\infty} + \frac{d\delta^*}{dx} \tag{67}$$

[6] The constant of proportionality is obtained empirically from reference 29.

Since equation (60a) gives the experimental result

$$\frac{d\delta^*}{dx} \approx 0.08(x - x_o)^{-0.39} \tag{68}$$

it is clear that the power-law approximation to $\overline{Y}(x)$ will lie between 0.70 (if the $\overline{V^*}$-term dominates in eq. (67)) and 0.62 (if the δ^*-term dominates). In fact, if the proportionality constant of equation (35) is determined from the data at $x = 102$ inches,

$$\overline{V^*} \approx 0.5\sqrt{\nu\xi'} \tag{69}$$

If this is used with equations (67) and (68) to predict

$$\overline{Y}(x) \approx 0.18(x - x_o)^{0.65} \tag{70}$$

the agreement with the directly measured result, equation (62), is good.

It should be remarked parenthetically that, although adequate measurements of $\gamma(x,y)$ are still not available on the smooth-wall turbulent boundary layer, an indirect verification of equations (34) and (35) follows from approximate agreement between the experimental (or analytically inferred) $\delta(x)$ and the predicted $\sigma(x)$ and $\overline{Y}(x)$, using reasoning like that presented in detail for the rough-wall case.

TWO-DIMENSIONAL WAKE

The measurements of Townsend (ref. 10) in the plane wake far behind a circular rod provide another case in which equations (34) and (35) can be checked against experiment.

From conservation of momentum and the assumption of similarity, dimensional reasoning yields the experimentally verified predictions that far behind the obstacle a turbulent wake spreads parabolically ($\delta \propto x^{1/2}$) and that the characteristic mean velocity defect decreases parabolically ($(\overline{U}_\infty - \overline{U}_o) \propto x^{-1/2}$) (ref. 30). This means that the plane wake is a constant Reynolds number shear flow and therefore significantly simpler than, for example, the boundary layer.

Far behind the wake-producing obstacle, where the fully developed wake is finally reached, the difference between minimum and maximum velocity is so small that equation (67) can be approximated by

$$\frac{d\overline{Y}}{dx} \approx \frac{\overline{V^*}}{\overline{U}_\infty} \tag{71}$$

Since there are only two points in the fully developed x-range, it has not been possible to determine empirical power laws for δ, $\overline{Y}$, and σ. The pertinent experimental result is simply that within the experimental uncertainty the points in the fully developed range are consistent with parabolic growth for all three lengths.

Verification of equation (34) again requires data on $\frac{v'}{\overline{U}}(x)$ and $L_L(x)$. As can be anticipated for a constant Reynolds number flow, the root-mean-square turbulent velocities are proportional to the characteristic mean velocity (mean velocity difference in the wake) so that $v' \propto x^{-1/2}$. In this asymptotic state, the mean velocity differences are all

small $\frac{\overline{U}_\infty - \overline{U}_o}{\overline{U}_\infty} \ll 1$ so that $\overline{U} \approx \text{Constant} \approx \overline{U}_\infty$. Furthermore, constant Reynolds number implies Lagrangian scale proportional to Eulerian scale ($L_L(x) \propto L(x)$), and with the general assumption of $L \propto \delta$ it follows that $L_L \propto x^{1/2}$. Equation (34) then gives as prediction for the variation in wrinkle amplitude of the turbulence front

$$\sigma(x) \propto x^{1/2} \tag{72}$$

in agreement with the directly measured result, in the similarity (large x) zone.

For the comparison of equation (35) with experiment, no data on ξ' are available. As in the boundary layer, it will therefore be assumed that $\xi' \propto v'/\lambda$. Since $v' \propto x^{-1/2}$ and $\lambda \propto x^{1/2}$, equation (35) predicts

$$\overline{V^*} \propto x^{-1/2} \tag{73}$$

whence

$$\overline{Y} \propto x^{1/2} \tag{74}$$

again in agreement with the directly measured result.

ROUND JET

Since fairly detailed turbulence data were already available for the case of the round turbulent jet (refs. 2 and 31) entering fluid at rest, intermittency surveys $\gamma(x,r)$ have been made during the course of this investigation to provide further experimental check on the proposed physical picture of the turbulence front.

From conservation of momentum and the assumption of similarity dimensional reasoning yields the experimentally verified predictions that far from its source the round turbulent jet spreads linearly ($r_{1/2} \propto x$) and that the characteristic mean velocity decreases hyperbolically ($\overline{U}_o \propto x^{-1}$) (ref. 30). Thus, the round jet is another constant Reynolds number flow and therefore relatively simple.

The new measurements made in the course of this study (fig. 24) give as power-law approximations with the "best" common origin,

$$r_{1/2} \propto \left(\frac{x}{d} - 3\right)^{1.00 \pm 0.05} \tag{75}$$

$$\overline{R} \propto \left(\frac{x}{d} - 3\right)^{0.88 \pm 0.05} \tag{76}$$

$$\sigma \propto \left(\frac{x}{d} - 3\right)^{1.06 \pm 0.05} \tag{77}$$

which may all be taken as linear within the experimental uncertainty.

Previous measurements have shown $v'/\overline{U}$ to be constant and independent of x at corresponding radical positions in the jet. Furthermore, the constancy of Reynolds number again permits the inference that $L_L \propto L$. With the assumption that $L \propto r_{1/2}$, equation (34) predicts

$$\sigma \propto (x - x_o) \tag{78}$$

in reasonable agreement with equation (77).

For the $\overline{V^*}(x)$ evaluation it is again assumed that $\xi' \propto v'/\lambda$. With $v' \propto (x - x_o)^{-1}$ and $\lambda \propto L \propto r_{1/2} \propto (x - x_o)$ equation (35) gives

$$\overline{V^*} \propto (x - x_o)^{-1} \tag{79}$$

and the comparison with experiment can be made by using equation (79) to predict $\overline{R}(x)$, merely replacing $\overline{Y}$ by $\overline{R}$ in equation (65). Instead of attempting a detailed proper calculation only a rough estimate was made by assuming

$$\overline{V}(x,\overline{R}) \propto \overline{U}(x,\overline{R}) \propto \overline{U}(x,0)$$

Then the prediction is

$$\overline{R}(x) \propto (x - x_o) \tag{80}$$

in reasonable agreement with equation (76). In fact, a belief in full similarity for constant Reynolds number shear flows suggests that equation (80) may be more nearly correct than equation (76).

INTERMITTENCY AND MEASURED MEAN QUANTITIES

As pointed out earlier in the section on "Inference of Turbulence Properties From Intermittent Signal," there seems to be only a restricted likelihood of extracting from the measured statistical characteristics of the intermittent signal respectable quantitative results on the statistical properties of the turbulent flow in the convex bulges of the turbulent front. Probably the broadest obstacle to simple physical interpretation of results computed from equation (53) or (57) is the lack of homogeneity within a fully turbulent zone supporting transfer.

Nevertheless, it seems worth while to present, for some fluctuating variables which are zero in the potential fluid (i. e., satisfy the first requirement), the results of applying these two operators.

No detailed quantitative information has yet been obtained on the mean-value jump for any physical variable. A rough check from $u(t)$ oscillograms in the rough-wall boundary layer where $\gamma \approx 0.4$ indicated that the jump in longitudinal velocity was about 5 to 10 percent of $\overline{U}_\infty$.

Unfortunately, this still does not permit calculation of $\overline{u_T^2}$ because all velocity fluctuations violate the first condition; that is, they are nonzero in the potential flow.

For ξ-vorticity, which does satisfy this first condition, no mean-value jump is observable on the oscillograms. This is not surprising since this x-component has no corresponding mean vorticity in this flow field. It may be anticipated that the z-component ζ will be found to have a jump, if and when it is measured. A plot of $\overline{\xi_T^2} \equiv \overline{\xi^2}/\gamma$ is given in figure 30. To insure y-coordinate consistency, this particular $\gamma(y)$ has been measured with the vorticity meter as sensing element. It does not differ appreciably from $\gamma(y)$ as determined from the differentiated signal of a u-meter.

In the outer part of the intermittent zone $\overline{\xi^2}/\gamma$ turns out to be roughly constant, leading to the possible conclusion that $\overline{\xi^2}$ is relatively homogeneous in the turbulent fluid.

The Reynolds shear stress $-\rho\overline{uv}$ has been inferred to be zero in the potential field outside a turbulence front. Therefore, it may also be interesting to estimate $-\rho\overline{u_T v_T}$.

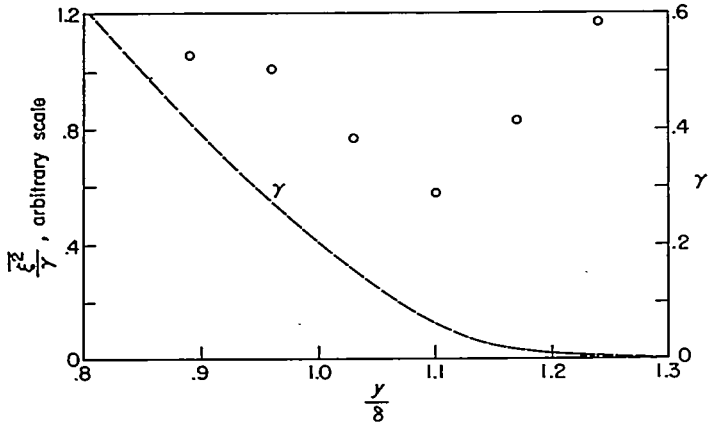

FIGURE 30.—Distribution of mean-square vorticity fluctuation divided by intermittency in boundary layer at $x=102$ inches.

Using a representation like equation (54) for $u(t)$ and $v(t)$ separately and assuming (a) no mean jump in $v(t)$, (b) $\overline{u_T b}=\overline{v_T b}=0$, and (c) $\overline{b^2 u_T v_T}=\overline{b^2}\,\overline{u_T v_T}$, it follows that

$$\overline{u_T v_T}=\frac{\overline{uv}}{\gamma} \tag{81}$$

Townsend (ref. 28) has plotted $\overline{uv}\Big/\gamma\dfrac{\partial\overline{U}}{\partial y}$ versus y without attempting a justification.

Figure 31 shows the result of applying equation (81) to the measured Reynolds shear stress in the rough-wall boundary layer and in Townsend's plane wake (ref. 10). The nonconstancy of $\overline{uv}/\gamma$ can probably be attributed largely to nonhomogeneity within the turbulent field.

In concluding this section it may be remarked that, if an existing nonhomogeneity for any variable in the turbulent part of the field depends only upon distance in from the front, a first-order estimate of its effect can be made by computing the average value generated at a fixed point by random motion of a "fixed" pattern like that in sketch (e).

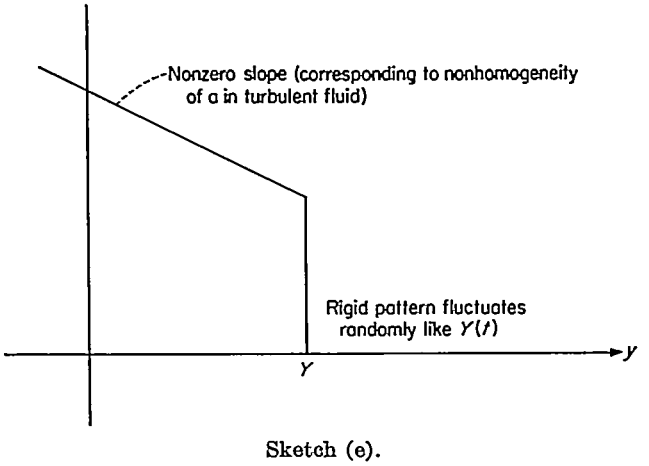

Sketch (e).

STATISTICAL DESCRIPTION OF TURBULENCE FRONT

The position of the turbulence front $Y(x,t)$ is a random variable stationary in time and nonstationary in x. The purpose of this section is to report some further measurements which have been made on its statistical properties, especially those of $Y(t)$ for a fixed value of x. Earlier

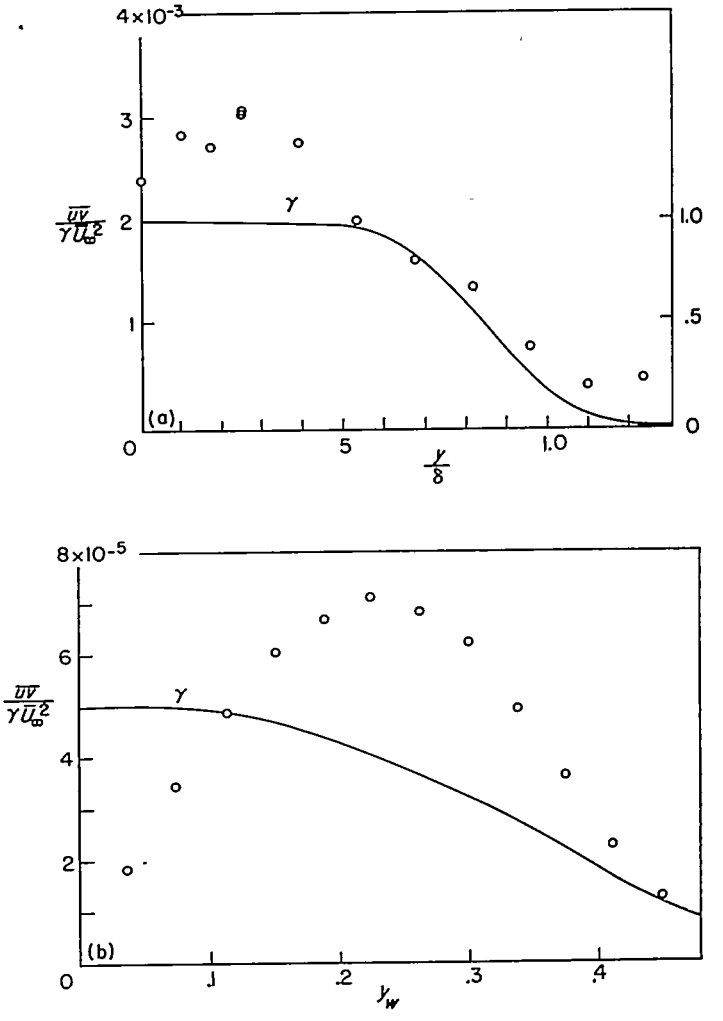

(a) Boundary layer at $x=102$ inches.
(b) Plane wake at $x=800$ inches. (Data from ref. 10.)

FIGURE 31.—Distributions of Reynolds shear stress divided by intermittency.

sections have emphasized its statistical variation with x, particularly through $\overline{Y}(x)$ and the standard deviation $\sigma(x)$.

It is of course possible for Y to be a multiple-valued function (see, e. g., fig. 1), but in most flows the occurrence of multiple values appears to be sufficiently rare that a discussion predicated upon a single-valued Y is applicable with good accuracy. This is especially true for the boundary layer, where turbulence levels tend to be appreciably lower than, for example, in jets entering a still medium. This conceptual restriction to single-valued Y, exercised throughout the report, will be justified empirically for the boundary layer by showing that the average wave length is considerably greater than the average wrinkle amplitude.

As a stationary random function $Y(t)$ is susceptible of quantitative statistical description in various ways, not all independent. Perhaps the two most common mutually independent functional representations for such variables are the autocorrelation function (or its Fourier transform, the power spectrum) and the probability density (or its Fourier transform, the characteristic function). Usually the lower order moments of the density and spectral functions, which have simple physical interpretations, are the most easily measured statistical properties.

The problem of acquiring detailed statistical information on $Y(t)$ is novel in the sense that nowhere in the experiment is there a signal which is simply proportional to the stationary variable under study. Therefore, the conventional statistical functions (above) are not readily measurable by standard techniques. It is fortuitous that the dissimilar character of the fields on opposite sides of $Y(t)$ gives such a convenient method of measuring probability density. However, the autocorrelation or power spectrum apparently cannot be directly measured, and therefore other direct statistical data have been sought, in particular, the probability density of "pulse lengths," actually the statistical measure of the times between successive occurences of any particular value of the primary variable $Y(t)$.

A challenging problem in the theory of stochastic processes is that of relating (if possible) these densities to the more conventional statistical measures. Up to the present time, only a few fringe results seem to have been obtained by workers in the field; these will be mentioned in appropriate context.

PROBABILITY DENSITY OF $Y(t)$

As has been pointed out in the "Introduction" (eq. (1)), the intermittency factor $\gamma(y)$ is simply the distribution function of $Y(t)$ and, therefore, $\partial\gamma/\partial y$ is its probability density.

Calculation of $\partial\gamma/\partial y$ shows that, except in the two tails of the function, it is remarkably symmetrical. Furthermore, the physical picture given here of front wrinkling as primarily a (Lagrangian) turbulent diffusion phenomenon then suggests a check to see how nearly $\partial\gamma/\partial y$ approximates a Gaussian function, since studies of scalar diffusion in isotropic turbulence have shown a closely Gaussian density. Figure 32 shows this check. It includes typical plots on

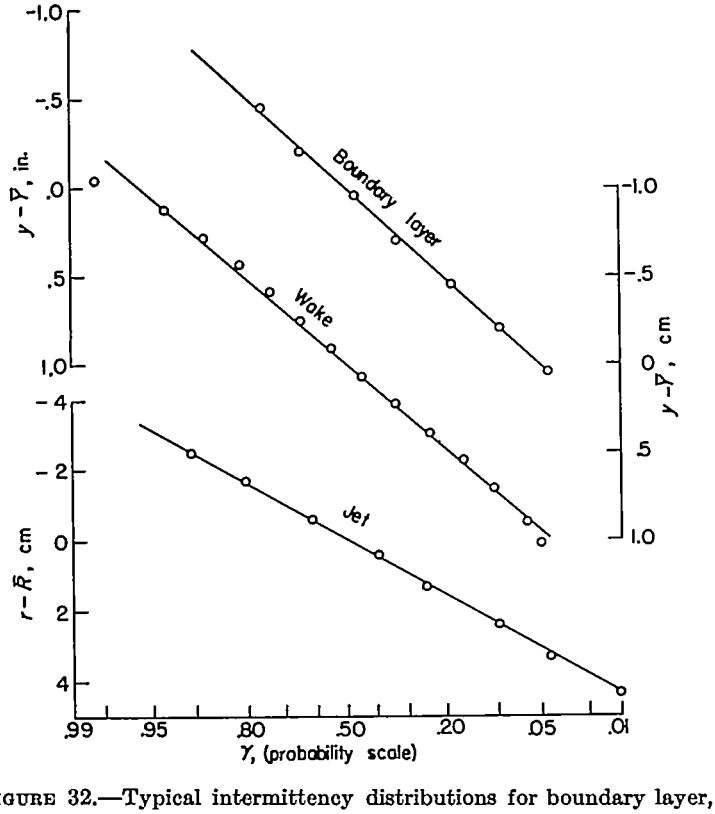

FIGURE 32.—Typical intermittency distributions for boundary layer, jet, and wake plotted on Gaussian probability scale.

Gaussian paper of $\gamma(y)$ for the boundary layer and for Townsend's wake, as well as $\gamma(r)$ for the round jet. Clearly all three distributions are Gaussian within the experimental precision except in the tail regions.

Deviations from symmetry must, of course, occur at the tails since the boundary conditions on the two sides are vastly different.

Since the nearly Gaussian character of dispersion in isotropic turbulence is still unexplained theoretically, it is not to be expected that this much more complex phenomenon can be clarified at present. Also, it must be emphasized that even in the former case it is not necessarily true that the probability densities are precisely Gaussian; the current conclusion is only that a Gaussian curve fits the data as closely as present experimental techniques produce data. Very likely it is the deviations (however small) which, when measured, will shed more light upon the central property of turbulence, the nonlinearity.

Batchelor (ref. 32) has pointed out that the Gaussian dispersion pattern observed at very large distances downstream from a contaminant source in a turbulent flow may be simply a consequence of the central limit theorem,[7] since the relative position of a fluid particle a long time after tagging may be regarded as the sum (time integral) of a large number of small displacements, which are at least uncorrelated for moderate intervals if not exactly statistically independent. In fact, if this reasoning does apply, it is doubly effective: Particle displacement, the principal variable, is itself the integral of particle velocity, so that the long-time displacement is the sum of a collection of sums.

Apparently, the central limit theorem has not been extended to integrals of continuous random variables, but some pertinent work has been done by Kac and Siegert (ref. 33), who showed mathematically that passage of a particular skew (probability density) random signal through a low-pass filter reduces the skewness. This prediction has been experimentally verified by Jastram (ref. 34) and by Iribe (ref. 35) A low-pass filter is, of course, qualitatively equivalent to integration.

PROBABILITY DENSITY OF PULSE LENGTHS

Experimental results.—From a sketch of $Y(t)$ as a stationary random variable, it is easily seen that the intermittent signal from a fixed probe provides a direct means of measuring the statistical distribution of the time intervals between successive occurrences of any particular value of Y.

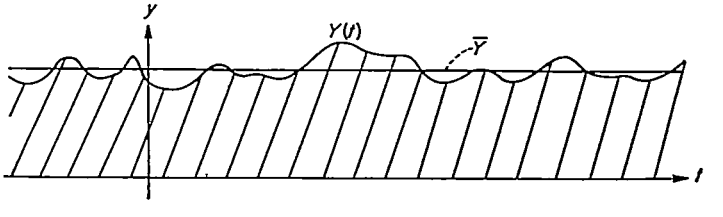

Sketch (f).

[7] In effect, this states that the sum of a number of statistically independent random variables approaches Gaussian character as the number increases without limit (provided that no finite group dominates the sum).

From the fluid-mechanical point of view this gives a convenient measure of the wave lengths of the mountains and valleys in the turbulence front. The laminar superlayer is thin enough to be considered a discontinuity in all of this analysis.

If T_1 is the duration of the probe in a turbulent zone and T_2, the duration in a nonturbulent zone, figure 29 gives the probability densities $p_1(T_1)$ and $p_2(T_2)$ at three different values of transversal position, that is, three different values of the intermittency factor.

By definition (of probability density), the curves in figure 29 are normalized to unit area. A check on their accuracy is given by the more or less obvious condition

$$\frac{\overline{T}_1}{\overline{T}_1+\overline{T}_2}=\gamma \tag{82}$$

where $\overline{T}_1=\int_0^\infty T_1 p_1(T_1)dT_1$ and $\overline{T}_2=\int_0^\infty T_2 p_2(T_2)dT_2$.

The terms $\overline{T}_1$ and $\overline{T}_2$ are average pulse durations in units of time and are functions of y or, alternatively, of γ since $\gamma(y)$ is monotonic.

The computations from figure 29 give (for $\delta\approx 3.5$ inches):

y/δ	γ directly measured	$\overline{T}_1$, sec	$\overline{T}_2$, sec	γ from $\overline{T}_1$ and $\overline{T}_2$	l_1, in.	l_2, in.
0.72	0.75	0.0155	0.0060	0.72	7.0	2.7
0.85	0.50	0.0106	0.0082	0.56	4.8	3.7
0.98	0.25	0.0069	0.0132	0.34	3.1	5.9

where $l_1\equiv\overline{U}_\infty\overline{T}_1$ and $l_2\equiv\overline{U}_\infty\overline{T}_2$ are approximate measures of the spatial extension of the average intervals in this x vicinity. This interpretation of the l's as average intercept lengths for the random variable $Y(x)$ gets increasingly accurate as the velocity fluctuation level decreases. This time-space transformation is, in fact, identical with that first proposed by Taylor for an isotropic turbulence (ref. 36) and discussed in more detail by others (refs. 37 and 18).

A comparison between $\frac{1}{2}(l_1+l_2)$ for $\gamma=0.50$ and the standard deviation σ of $Y_1(t)$ at the same x-station gives a rough measure of the flatness of the wrinkled turbulence front. For this particular station in the boundary layer,

$$\frac{2\sigma}{l_1+l_2}\approx 0.13 \tag{83}$$

which indicates a rather flat front, as assumed in the earlier theoretical discussion on the propagation of the laminar superlayer.

Inspection of figure 29 shows the following traits of the data:

(a) The points are rather scattered.

(b) For $\gamma=0.50$, p_1 and p_2 show an appreciable difference.

(c) The $\gamma=0.25$ and $\gamma=0.75$ cases, which might be expected to have identical curves with reversed labels, show this character qualitatively, though not accurately.

Properties (b) and (c) can apparently be attributed chiefly to the shortness of oscillographic samples;[8] therefore, the curves in figure 29 have been labeled with the γ's actually given by these short samples, and the apparent discrepancies (b) and (c) are qualitatively explained. In other words, a short sample with actual $\gamma=\gamma_1$ drawn from an infinite record with $\gamma=\gamma_2$ can be expected to show other statistical properties resembling those of an infinite record with $\gamma=\gamma_1$.

Two other sources of uncertainty in the data of figure 29 are (1) the natural uncertainty of measurement in the presence of noise, even with perfect equipment, and (2) imperfections in measuring equipment and techniques.

The first of these difficulties affects all intermittency measurements and is basically insurmountable. Of course, the noise level could be reduced somewhat and, under simplifying statistical assumptions on both noise and signal, some estimate of the effect could be made.

The second difficulty probably affects p_1 and p_2 measurements more seriously than direct γ measurements. For example, suppose that the measuring process misses a sizable number of the shortest turbulent bursts. This fault will scarcely affect the directly measured γ since these contain only a small part of the total number of pulses to be counted (except for $\gamma\ll 1$). On the other hand, this fault will not only change the character of $p_1(T_1)$ for small values of T_1 but also will change the level of $p_2(T_2)$ for large values of T_2, since the very short turbulent bursts subdivide long potential bursts into shorter ones. Hence, this fault will seriously affect $\overline{T}_2$ and, therefore, γ as computed from $\overline{T}_1$ and $\overline{T}_2$. Precisely this fault is observable on the oscillographic traces.

Other defects similarly observed are the (relatively infrequent) missing of short potential bursts and the occasional overhang of the trigger signal beyond the duration of a turbulent burst. The last of these faults affects the direct γ measurement as well.

An obvious way around some of these difficulties is the direct use of $\xi(t)$ or $\frac{\partial u}{\partial t}(t)$ oscillograms to compute p_1 and p_2. To some extent this was done, and the extreme tediousness of this method is exactly why the samples processed are so short.

This inadequate sample length (fault (3)) most seriously affects the results in the large T_1 and T_2 ranges. The relative seriousness of this limitation for long versus short pulses is not given (as might be guessed at first blush) by the ratio of sample length to pulse length but by the ratio of sample length to the inverse of the frequency of occurrence of the particular length of pulse (actually a small range) in question. For example, in a 3-second oscillographic sample, the points on the tails of p_1 and p_2 may represent as few as one or two actual occurrences. With this in mind it can be concluded that the agreement between values of γ obtained via $\overline{T}_1$ and $\overline{T}_2$ and values of γ directly measured is surprisingly good.

It would be interesting to know whether p_1 and p_2 approximate exponential distributions for large values of T_1 and T_2. However, the uncertainty of the points in just this range is so great as to render such a quantitative question unanswerable. Some very indirect evidence via the power spectrum of the Schmitt trigger output for $\gamma=0.50$ will be discussed in a following section.

Since the small T_1 and T_2 ranges of p_1 and p_2 are quite uncertain (i.e., for bursts shorter than 2 milliseconds), some

[8] About 3 seconds, as compared with the 2 minutes used in obtaining the γ's directly.

qualitative analytical consideration of the anticipated behavior in this range is in order. These short segments arise whenever the hot-wire passes just below a local maximum (for turbulent fluid) or just above a local minimum (for potential fluid) in $Y(t)$.

The variable $Y(t)$ must be differentiable (since it occurs in a continuum); therefore, its extremes have horizontal tangents. Thus, a Taylor series expansion of $Y(t)$ about any local extreme $t=t_m$ starts with a term proportional to $(t-t_m)^2$. The limiting behavior of p_1 and p can thus be obtained by considering a parabola $C=D^2$ as in sketch (g). The problem is then as follows: Suppose C has a flat probability density $p_C(C)$;[9] what is the probability density p_D of $D=\sqrt{C}$?

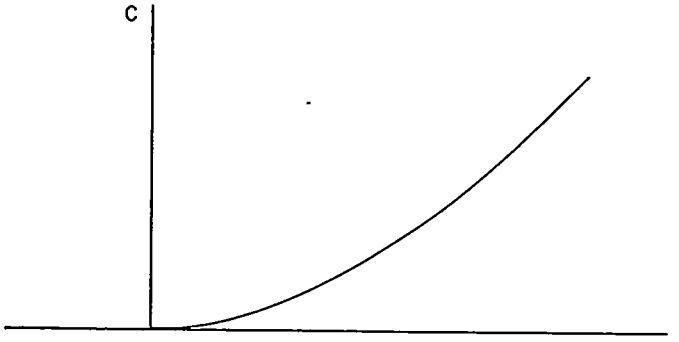

Sketch (g).

In general, if $C=C(D)$ is unique,

$$p_D(D)=p_C(C)\frac{dC}{dD} \tag{84}$$

whence, for this particular problem

$$p_D(D) \propto D \tag{85}$$

It follows from this calculation that *the probability density of the intervals between successive occurrences of any particular value of a differentiable random variable must start out (a) from the origin and (b) linearly.* Specifically, $p_1(T_1)$ and $p_2(T_2)$ must behave in this fashion, even though the measured curves do not all show this tendency in the range covered.

By reasoning similar to the above it is obvious that for a continuous but nondifferentiable variable (corresponding to pointed but uncusped extremes) the corresponding density starts out at a finite value.

Status of random-variable theory.—The mathematical problem of relating the probability density of the intervals between successive occurrences of any particular value of a continuous random variable to the ordinarily more accessible statistical functions (probability density of the primary variable, power spectrum, etc.) has apparently not been solved, even for a Gaussian variable.

Rice (ref. 38) has deduced the probability of a zero of a Gaussian variable $I(t)$ in an interval $(t_1+t_2),(t_1+t_2+dt)$ when there is a zero at t_1. However, the probability density of intervals between successive zeros (or successive occurrences of any other particular value) does not appear to follow easily from Rice's result. Of course, in the particular case when successive intervals are statistically independent, the occurrence numbers have a Poisson density, and the interval lengths have a simple exponential probability density.

A more directly applicable result, apparently due to Rice (ref. 38), relates the expected rate of occurrence of any particular value of a Gaussian variable $I(t)$ to the probability density of the variable and the autocorrelation function behavior in the vicinity of zero:

$$N_I=\frac{e^{-\frac{I^2}{2\psi(0)}}}{\pi}\left[-\frac{\psi''(0)}{\psi(0)}\right]^{1/2} \tag{86}$$

where $\psi(\tau)$ is the nonnormalized autocorrelation function $\overline{I(t)I(t+\tau)}$ and a prime indicates differentiation. The proof of equation (86) requires also that $I(t)$ and $I'(t)$ be uncorrelated—which is automatically satisfied for a stationary variable.

However, it must be emphasized that the pristine simplicity of this theorem is dependent upon the restriction to a Gaussian variable. Two of the seemingly inexhaustible number of fortuitous properties of the Gaussian probability density are:

(a) If a variable is Gaussian, so is its derivative.

(b) If two Gaussian variables are uncorrelated, it follows that they are statistically independent.

Without these built-in conveniences, it seems likely that such a theorem could be deduced only with the general assumptions that the variable and its derivative are statistically independent.

For the expected rate of zeros, equation (86) reduces to (ref. 38)

$$N_0=\frac{1}{\pi}\left[-\frac{\psi''(0)}{\psi(0)}\right]^{1/2} \tag{87}$$

Equation (87) has been used by Liepmann, Laufer, and Liepmann (ref. 39) to measure the microscale in a decaying isotropic turbulence. It will be used here to obtain $\psi''(0)$ for the turbulence front $Y(t)$.

Measurements have also been made of the average rate of occurrence of the values of $Y(t)$ corresponding to $\gamma=0.25$ and 0.75 in the intermittent zone of the rough-wall boundary layer. In figure 33, the three experimental points are compared with equation (86). The $\frac{y-Y}{\sigma}$ location of the three experimental points has been chosen according to the value of γ of the short samples (from which the $N's$ were measured; see the preceding table) rather than the true physical locations of the probe. The agreement is better than can be expected with the uncertainty of the measurements and therefore fortuitous. The number given for the rate of occurrence of zeros, $N_0 \approx 108$ per second, is interpolated along the Gaussian curve.

Measurements of the probability density of zeros in the fluctuating part of the signal from a human voice have been reported by Davenport (ref. 40).

[9] The very small range to be studied, that is, just the immediate vicinity of an extreme, permits approximating any small segment of a finite probability density by a constant value.

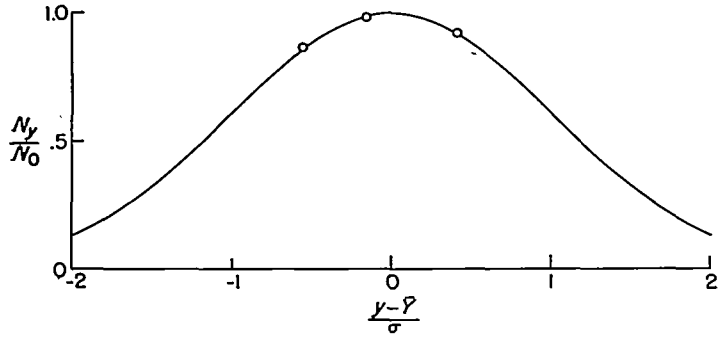

FIGURE 33.—Frequency of occurrence of zero and two other particular values of $Y_1(t)$ in boundary layer at $x=102$ inches. Solid curve is that of a strictly Gaussian variable. $N_0=108$.

POWER SPECTRUM OF SCHMITT TRIGGER OUTPUT

As indicated in figure 6, the output of the Schmitt trigger is in principle a random flat-top signal which is on whenever the probe is in turbulent fluid and off whenever it is in potential flow. Obviously the statistical properties of this signal must have some relation to those of the primary variable $Y(t)$, and therefore two convenient properties have been measured. The first is the probability density of pulse lengths, tops and bottoms separately; these are, of course, just $p_1(T_1)$ and $p_2(T_2)$ (fig. 29). The second is the power spectrum of the trigger output, measured at the same locations as the densities (fig. 28).

The three spectra have the same general shape, with power-law decrease for high frequency as indicated in the figure.

It might be expected that a relation should exist between the pulse-length densities of any flat-top signal and its power spectrum, but a search of the literature has uncovered no such analytical results except in special cases, one of which is used below.

The simplest of the three signals is that corresponding to $\gamma=0.50$, and in figure 28 this power spectrum is seen to agree closely with that for a "Poisson type" flat-top signal (see, e. g., ref. 38):

$$F(n)\propto\frac{M}{M^2+\pi^2n^2} \tag{88}$$

where M is the average number of jumps per second and n is cyclic frequency. For this application and $\gamma=0.50$, $M\neq N_0$, the average number of zeros per second in $Y-\overline{Y}$, since the distribution of zeros cannot be truly Poisson.

The very good agreement in figure 28 implies only that in this case $p_1(T_1)$ and $p_2(T_2)$ could be exponential away from the origin, even though the directly measured data are too uncertain to permit any estimates. However, no assertion can be made, since the -2 power spectral decrease is characteristic of most signals with "discontinuities."

AUTOCORRELATION FUNCTION OF $Y(t)$

The approximately Gaussian character of $Y-\overline{Y}$ permits application of equation (87) relating the zero occurrence rate and the autocorrelation. For this purpose the nonnormalized autocorrelation is defined by

$$\psi(\tau)\equiv\overline{Y_1(t)Y_1(t+\tau)} \tag{89}$$

where $Y_1\equiv Y-\overline{Y}$. Obviously $\psi(0)=\sigma^2$ and, since N_0 and σ are the measured quantities, equation (87) is written

$$\psi''(0)=-\pi^2\sigma^2N_0^2 \tag{90}$$

where

$$N_0=\frac{2}{\overline{T_1}+\overline{T_2}}\text{ zeros/sec} \tag{90a}$$

For the rough-wall turbulent boundary layer at $x=102$ inches, $\sigma=0.55$ inch and $N_0=108$ zeros per second, so

$$\psi''(0)=3.4\times10^4\text{ sq in./sec}^2 \tag{91}$$

A corresponding characteristic length mathematically equivalent to the dissipative scale (microscale) in turbulence can be deduced by the time-space transformation mentioned earlier:

$$\lambda_Y=\overline{U}_\infty\left[\frac{2\psi(0)}{\psi''(0)}\right]^{1/2}=\frac{\sqrt{2}\,\overline{U}_\infty}{\pi N_0} \tag{92}$$

For this particular case,

$$\lambda_Y\approx1.9\text{ in.} \tag{93}$$

which is a bit smaller than l_1 and l_2 in the preceding table for $\gamma=0.50$.

For low turbulence levels, one might expect the quantity $\frac{v'}{\overline{U}}\lambda_Y$ to be of the order of the Lagrangian spatial microscale $\lambda_s=\lambda_t v'$ (ref. 18), which is roughly equal to the Eulerian microscale λ over a wide range of R_λ in isotropic turbulence (ref. 18). In this case, $\left(\frac{v'}{\overline{U}}\lambda_Y\right)\approx0.09$ inch. This is the same order as λ in the neighboring turbulence. Since R_λ for this turbulence is roughly 70, which (in isotropic turbulence) gives $\lambda_s\approx1.5\lambda$, the conclusion here is that

$$\frac{v'}{\overline{U}}\lambda_Y\approx v'\lambda_t \tag{94}$$

or, since $\overline{U}\approx\overline{U}_\infty$, the Lagrangian time mocroscale of the neighboring turbulence is given roughly by

$$\lambda_t\approx\frac{\sqrt{2}}{\pi N_0} \tag{95}$$

Equation (90) gives only the vertex curvature of the autocorrelation function. Because of the Gaussian character of $Y(t)$, it is possible to estimate the entire $\psi(\tau)$ from the spectrum of the trigger output. It has been shown by North (see ref. 41) that the autocorrelation function of a strongly clipped Gaussian variable is simply related to the autocorrelation function of the variable itself:

$$\frac{\psi_c(\tau)}{\psi_c(0)}=\frac{2}{\pi}\sin^{-1}\left[\frac{\psi(\tau)}{\psi(0)}\right] \tag{96}$$

A strongly clipped variable is just a flat-top signal which changes sign whenever the primary variable passes through zero—which exactly describes the relation between the trigger output and the primary variable $Y(t)$.

Since, as shown by Wiener (ref. 42), the autocorrelation function of a stationary random variable is just the Fourier cosine transform of its power spectrum (and vice versa),

$$\psi_c(\tau)=\int_0^\infty F_c(n)\cos 2\pi n\tau\, dn \tag{97}$$

$$F_c(n)=4\int_0^\infty \psi_c(\tau)\cos 2\pi n\tau\, d\tau$$

the autocorrelation of the trigger output is computed from the measured power spectrum. The good agreement of $F_c(n)$ with the form in equation (88) permits using a simple exponential for $\psi_c(\tau)$ (ref. 38):

$$\frac{\psi_c(\tau)}{\psi_c(0)}\approx e^{-2M\tau} \tag{98}$$

Then, equation (94) gives the autocorrelation function of the turbulence front location:

$$\frac{\psi(\tau)}{\psi(0)}\approx \sin\left(\frac{\pi}{2}e^{-2M\tau}\right) \tag{99}$$

which is plotted in figure 34. The vertex osculating parabola corresponding to $\psi''(0)$ as given by equation (87) and the directly measured zero occurrence rate are drawn in for comparison. The former parabola should give the origin behavior of $\psi(\tau)$ more accurately than equation (99).

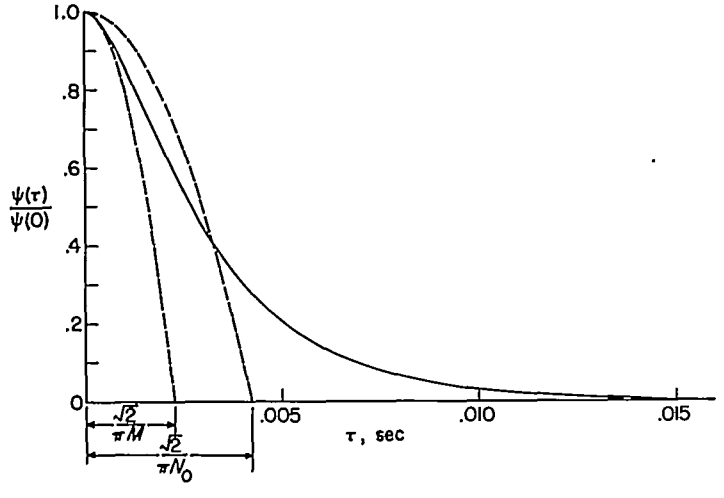

FIGURE 34.—Autocorrelation function of turbulence front location as a function of time in boundary layer at $x=102$ inches.

As should be expected, the calculation of $\psi''(0)$ for equation (99) gives

$$\frac{\psi''(0)}{\psi(0)}=-\pi M^2 \tag{100}$$

identical with equation (87), if $M\to N_0$.

In fact, it found experimentally that $M\approx 2N_0$ for this investigation. This is not surprising since the differentiability of $Y_1(t)$, whose zeros give the square-wave jumps, leads to a considerable deficit of short pulses as compared with a truly Poisson square wave (see the section "Experimental results" under "Probability Density of Pulse Lengths").

Of course, the power spectrum of $Y_1(t)$ could be calculated by taking the Fourier cosine transform of $\psi(\tau)$ but the data are sufficiently inaccurate that further manipulation scarcely seems worth while.

Other characteristic lengths of the wrinkled turbulence front can be estimated from the integral of $\psi(\tau)$, mathematically analogous to the integral scale of turbulence, but these may be less pertinent than, for example, l_1 and l_2, the average pulse lengths:

$$\frac{1}{\psi(0)}\int_0^\infty \psi(\tau)\, d\tau=\frac{1}{2M\sigma^2}\int_0^{\pi/2}\frac{\sin p}{p}\, dp\equiv\frac{Si\left(\frac{\pi}{2}\right)}{2M\sigma^2} \tag{101}$$

whence,

$$\frac{\overline{U}_\infty}{\psi(0)}\int_0^\infty \psi(\tau)\, d\tau=7.4\,\text{in.}$$

which turns out to be the same order as l_1 and l_2.

Alternatively,

$$\frac{v'}{\psi(0)}\int_0^\infty \psi(\tau)\, d\tau=0.35\,\text{in.}$$

both values being for the rough-wall boundary layer at $x=102$ inches.

CONCLUDING DISCUSSION

From the analytical and experimental results reported here on the problem of the relatively sharp instantaneous front separating turbulent fluid from nonturbulent fluid (as at a free-stream boundary), the following new conclusions are drawn:

1. The nonturbulent region is a field of irrotational fluctuations.

2. The front separating turbulent from potential flow is actually a very thin fluid layer in which viscous forces are of primary importance. The role of this "laminar superlayer" is the propagation of vorticity (both mean fluctuating) into the potential field. It is maintained thin by propagation relative to the fluid and by the random stretching of vortex lines in its local vorticity gradient.

3. The common occurrence of contiguous rotational and irrotational velocity fluctuation fields underscores the usefulness of confining the word "turbulent" to random rotational fields only.

4. The rate of increase of wrinkle amplitude of the turbulence front can be roughly predicted in terms of a Lagrangian diffusion analysis, using the statistical properties of the turbulence in the fully turbulent zone. The actual estimate is given by equation (34).

5. By dimensional reasoning and, independently, through a model of the laminar superlayer, the thickness of the superlayer can be estimated. The simplest approximation is equation (51), giving a thickness of the same order as the Kolmogoroff (minimum) turbulence length.

6. The propagation velocity $\overline{V^*}$ of the turbulence front is taken by dimensional reasoning to be proportional to $\sqrt{\nu\xi'}$. This is roughly verified by experiment.

7. The downstream rate of growth of the turbulence front, as measured by standard deviation $\sigma(x)$ and transversal position $\overline{Y}(x)$, is found to be proportional to the shear-zone thickness, within the experimental precision, for plane wake, round jet, and rough-wall boundary layer. This is shown

independently by direct experiment and by application of the results outlined in the previous paragraphs.

8. The probability density of the turbulence front location at any fixed downstream station is Gaussian within the precision of the measurements everywhere except at the tails. This is found experimentally for all three types of turbulent shear flow studied.

9. The probability density of the pulse lengths in the intermittent signal deviates strongly from the simple exponential type, presumably because $Y(t)$ is differentiable.

10. The autocorrelation function of $Y_1(t)$ for the boundary layer is found very indirectly from experiment to be as shown in figure 34.

It seems likely that the presence of the turbulence front with its attendant detailed statistical properties will have to be included in basic research on turbulent shear flows with free-stream boundaries. It is not quite so clear that it must be explicitly included in semiempirical engineering estimates concerned only with overall transfer; so far no case has been encountered in which the front grows at a rate distinctly different from the gross shear-layer growth.

It appears that at present this new physical picture introduces at least as many new questions as it gives explanations of older observations. Insofar as it is concerned with a boundary condition, it tells nothing about transport phenomena within a turbulent region. Yet, since the wrinkle amplitude $\sigma(x)$ and transversal travel $\overline{Y}(x)$ of the turbulence front appear to be governed by (or related to) properties of the contiguous turbulence, any gross assumption on these variables implies consequent relations among the turbulence properties.

It should especially be pointed out that the present investigation does not appear to shed any light on the characteristic difference between transport rates of vector (momentum) and scalar (heat, mass) properties. In fact, since it is concluded that no mean momentum can be transported beyond the turbulence front it appears that (for laminar Prandtl and Schmidt numbers not very much smaller than unity) the front should apply equally well to heat or chemical composition. Oscillographic observations (not mentioned in the body of the report) in a hot jet show a temperature fluctuation intermittency, presumably coincident with the vorticity intermittency. If this inference is true, then the vector versus scalar transport rate difference will have to be explained in terms of properties of the entirely turbulent region.

Interesting speculations in this direction have been made by Townsend (ref. 10), who suggests that momentum is largely transported by relatively high wave number fluctuations while heat is transported by both low and high wave number fluctuations, that is, by jet convection and by gradient diffusion, respectively. However, there are two dubious minor postulates in his analysis (mentioned here in the section "Inference of Turbulence Properties From Intermittent Signal" and at the end of the section "Laminar Superlayer") and also he has not clarified the principal assumption vis-à-vis the known fact that the shear correlation $\overline{uv}$ appears to get ever increasing contributions toward the low wave numbers (ref. 43). Finally, his inference that the lateral jets (bulges) convect little longitudinal momentum appears to be in contradiction to the fact that the intermittent velocity signal shows an appreciably lower mean in the turbulent segments that in the potential ones, as seen in figures 9 and 15.

THE JOHNS HOPKINS UNIVERSITY,
BALTIMORE, MD., *January 20, 1953.*

APPENDIX

GROWTH OF ROUGH-WALL BOUNDARY LAYER

Although the growth of turbulent boundary layers with zero static-pressure gradient is better approximated by a logarithmic function (ref. 11), the exploratory purposes of this investigation are satisfied by the simpler and less accurate power-law treatment.

The momentum integral relation for turbulent boundary layer with zero static-pressure gradient can be written approximately as (ref. 11)

$$\frac{d\theta}{dx}=\frac{\tau_o}{\rho\overline{U}_\infty^2} \tag{A1}$$

The following rough assumptions are made:

(a) Simple geometrical similarity in mean velocity profiles:

$$\frac{\overline{U}}{\overline{U}_\infty}=fn\left(\frac{y}{\delta}\right)$$

(b) "Fully rough" wall conditions:

$$\frac{U_\tau h}{\nu}\geqq 100$$

Therefore,

$$\tau_o\propto\rho[U(h)]^2$$

where h is effective roughness height.

(c) Power-law velocity profile:

$$\frac{\overline{U}}{\overline{U}_\infty}=\left(\frac{y}{\delta}\right)^m$$

From assumptions (a) and (c)

$$\frac{\overline{U}(h)}{\overline{U}_\infty}=\left(\frac{h}{\delta}\right)^m \tag{A2}$$

whence the second assumption gives

$$\tau_o\propto\rho\overline{U}_\infty^2\left(\frac{h}{\delta}\right)^{2m} \tag{A3}$$

Since $\theta\propto\delta$, substitution of equation (A3) into equation (A1) gives

$$\frac{d\theta}{dx}\propto\theta^{-2m} \tag{A4}$$

for h=Constant. Therefore,

$$\theta\propto(x-x_o)^{\frac{1}{2m+1}} \tag{A5}$$

Equation (A5), a simple power law, permits approximation to the actual boundary-layer growth with accuracy adequate for the present investigation.

In fact, since both m and the exponent in equation (A3) have been measured independently, there is opportunity for an experimental check on the accuracy of the present crude approach: Mean velocity profiles (fig. 11) give $m\approx 1/3.5$. Therefore, the analysis predicts

$$\theta\propto(x-x_o)^{0.64}$$

whereas measurements of boundary-layer growth (fig. 12) give

$$\theta\propto(x-x_o)^{0.63\pm 0.1}$$

It should be pointed out that boundary layers in general cannot have simple geometrical similarity because their characteristic Reynolds numbers increase with x.

This particular "rough-wall" boundary layer is fully rough all the way downstream (from x=0 to x=102, $U_\tau h/\nu$ falls from 200 to 145), if the peak-to-peak height of the corrugation is interpreted as h.

REFERENCES

1. Taylor, G. I.: Statistical Theory of Turbulence. Parts I–IV. Proc. Roy. Soc. (London), ser. A, vol. 151, no. 873, Sept. 2, 1935, pp. 421–478.
2. Corrsin, Stanley: Investigation of Flow in an Axially Symmetrical Heated Jet of Air. NACA WR W–94, 1943. (Formerly NACA ACR 3L23.)
3. Liepmann, Hans Wolfgang, and Laufer, John: Investigations of Free Turbulent Mixing. NACA TN 1257, 1947.
4. Schubauer, G. B., and Klebanoff, P. S.: Investigation of Separation of the Turbulent Boundary Layer. NACA Rep. 1030, 1951. (Supersedes NACA TN 2133.)
5. Laufer, John: Investigation of Turbulent Flow in a Two-Dimensional Channel. NACA Rep. 1053, 1951. (Supersedes NACA TN 2123.)
6. Townsend, A. A.: Local Isotropy in the Turbulent Wake of a Cylinder. Australian Jour. Sci. Res., ser. A, vol. 1, no. 2, June 1948, pp. 161–174.
7. Charters, Alex C., Jr.: Transition Between Laminar and Turbulent Flow by Transverse Contamination. NACA TN 891, 1943.
8. Emmons, H. W.: The Laminar-Turbulent Transition in a Boundary Layer—Part I. Jour. Aero. Sci., vol. 18, no. 7, July 1951, pp. 490–498.
9. Mitchner, M.: The Propagation of Turbulence Into a Laminar Boundary Layer. Interim Tech. Rep. No. 3, Combustion Tunnel Lab., Harvard Univ., June 1952.
10. Townsend, A. A.: The Fully Developed Turbulent Wake of a Circular Cylinder. Australian Jour. Sci. Res., ser. A, vol. 2, no. 4, Dec. 1949, pp. 451–468.
11. Schlichting, Hermann: Grenzschicht-Theorie. G. Braun (Karlsruhe), 1951.
12. Corrsin, Stanley, and Uberoi, Mahinder S.: Spectra and Diffusion in a Round Turbulent Jet. NACA Rep. 1040, 1951. (Supersedes NACA TN 2124.)
13. Kovásznay, L. S. G.: Quarterly Progress Report of Aeronautics Department. Contract NOrd–8036–JHB–3D, The Johns Hopkins Univ., Jan. 1–Mar. 31, 1950.
14. Kistler, A. L.: The Vorticity Meter. M. S. Thesis, The Johns Hopkins Univ., June 1952.

15. Laufer, John: The Structure of Turbulence in Fully Developed Pipe Flow. NACA Rep. 1174, 1954. (Supersedes NACA TN 2954.)
16. Townsend, A. A.: The Structure of the Turbulent Boundary Layer. Proc. Cambridge Phil. Soc., vol. 47, pt. 2, Apr. 1951, pp. 375–395.
17. Taylor, G. I.: The Statistical Theory of Isotropic Turbulence. Jour. Aero. Sci., vol. 4, no. 8, June 1937, pp. 311–315.
18. Uberoi, Mahinder S., and Corrsin, Stanley: Diffusion of Heat From a Line Source in Isotropic Turbulence. NACA Rep. 1142, 1953. (Supersedes NACA TN 2710.)
19. Lessen, Martin: On Stability of Free Laminar Boundary Layer Between Parallel Streams. NACA Rep. 979, 1950. (Supersedes NACA TN 1929.)
20. Taylor, G. I.: Diffusion by Continuous Movements. Proc. London Math. Soc., ser. A, vol. 20, 1922, pp. 196–212.
21. Brier, G. W.: The Statistical Theory of Turbulence and the Problem of Diffusion in the Atmosphere. Jour. Meteorol., vol. 7, no. 4, Aug. 1950, pp. 283–290.
22. Batchelor, G. K.: Diffusion in a Field of Homogeneous Turbulence II. Proc. Cambridge Phil. Soc., vol. 48, pt. 2, Apr. 1952, pp. 345–362.
23. Frenkiel, F. N.: On Turbulent Diffusion. Rep. 1136, Symposium on Turbulence (June 1949), Naval Ord. Lab., July 1, 1950, pp. 67–86.
24. Corrsin, Stanley: Heat Transfer in Isotropic Turbulence. Jour. Appl. Phys., vol. 23, no. 1, Jan. 1952, pp. 113–118.
25. Clauser, F. H.: The Structure of the Outer Portion of Turbulent Shear Layers. Abstract of paper presented at Eighth Int. Cong. Theor. and Appl. Mech. (Istanbul, Turkey, Aug. 1952), June 1953.
26. Karlovitz, Bela, Denniston, D. W., Jr., and Wells, F. E.: Investigation of Turbulent Flames. Jour. Chem. Phys., vol. 19, no. 5, May 1951, pp. 541–547.
27. Prandtl, L.: The Mechanics of Viscous Fluids. Some Examples of Exact Solutions. Vol. III of Aerodynamic Theory, div. G, sec. 10, W. F. Durand, ed., Julius Springer (Berlin), 1935, pp. 61–69.
28. Townsend, A. A.: Momentum and Energy Diffusion in the Turbulent Wake of a Cylinder. Proc. Roy. Soc. (London), ser. A, vol. 197, no. 1048, May 11, 1949, pp. 124–140.
29. Corrsin, S.: Decay of Turbulence Behind Three Similar Grids. A. E. Thesis, C. I. T., June 1942.
30. Fluid Motion Panel of the Aeronautical Research Committee and Others (S. Goldstein, ed.): Modern Developments in Fluid Dynamics. The Clarendon Press (Oxford), 1938.
31. Corrsin, Stanley, and Uberoi, Mahinder S.: Further Experiments on the Flow and Heat Transfer in a Heated Turbulent Air Jet. NACA Rep. 998, 1950. (Supersedes NACA TN 1865.)
32. Batchelor, G. K.: Diffusion in a Field of Homogeneous Turbulence I. Australian Jour. Sci. Res., ser. A, vol. 2, no. 4, Dec. 1949, pp. 437–450.
33. Kac, M., and Siegert, A. J. F.: On the Theory of Noise in Radio Receivers With Square Law Detectors. Jour. Appl. Phys., vol. 18, no. 4, Apr. 1947, pp. 383–397.
34. Jastram, P. S.: The Effect of Nonlinearity and Frequency Distortion on the Amplitude Distribution for Stationary Random Processes. Ph. D. Dissertation, Univ. of Mich., 1947.
35. Iribe, P.: Some Properties of an Electronic Model of Turbulence. M. S. Thesis, The Johns Hopkins Univ., 1949.
36. Taylor, G. I.: The Spectrum of Turbulence. Proc. Roy. Soc. (London), ser. A, vol. 164, no. 919, Feb. 18, 1938, pp. 476–490.
37. Lin, C. C.: On Taylor's Hypothesis in Wind-Tunnel Turbulence. Memo. No. 10775, Naval Ord. Lab., Feb. 20, 1950; also, On Taylor's Hypothesis and the Acceleration Terms in the Navier-Stokes Equations. Quart. Appl. Math., vol. X, no. 4, Jan. 1953, pp. 295–306.
38. Rice, S. O.: Mathematical Analysis of Random Noise. The Bell System Tech. Jour., vol. 23, no. 3, July 1944, pp. 282–332; vol. 24, no. 1, Jan. 1945, pp. 46–108.
39. Liepmann, H. W., Laufer, J., and Liepmann, Kate: On the Spectrum of Isotropic Turbulence. NACA TN 2473, 1951.
40. Davenport, W. B., Jr.: Experimental Study of Speech-Wave Probability Distributions. Jour. Acous. Soc. Am., vol. 24, no. 4, July 1952, pp. 390–399.
41. Lawson, James L., and Uhlenbeck, George E. (eds.): Threshold Signals. First ed., McGraw-Hill Book Co., Inc., 1950, pp. 57–59.
42. Wiener, N.: Generalized Harmonic Analysis. Acta Math., vol. 55, 1930, pp. 117–258.
43. Corrsin, Stanley: An Experimental Verification of Local Isotropy. Jour. Aero. Sci., vol. 16, no. 12, Dec. 1949, pp. 757–758.